GFRJ – ATOM III Project

Team 31 Project Technical Report for the 2022 LASC

Igor S. Procopiak[1], Giulia F. Santos[2], Renan L. A. Mourão[3], Mylena C. P. B. N. Candido[4], Marcus V. A. Ribeiro[5], Matheus R. Fernandes[6], Igor F. S. R. Lopes[7], Lucas C. R. Fraga[8], Lucas J. Carneiro[9], Caio M. G. Burlini[10], Gabriel M. O. de A. Bastos[11]

Rio de Janeiro State University, Rio de Janeiro, Rio de Janeiro, 20550-900

This report presents the technical aspects of the GFRJ's project for 2022 Latin American Space Challenge that is competing in the 3km AGL apogee with solid rocket propulsion system category. *ATOM III*, the launch vehicle, has a M-class solid motor that uses potassium nitrate and sorbitol as its propellant. Its structure is made of fiberglass and aluminum, with its aerodynamics calculations made with *OpenRocket.* Its primary missions are the realization of a biological experiment, present inside Nose Cone, in addition to succeed in launch and recover the rocket.

I. Nomenclature

v_{ds}	=	drogue stage velocity
v_{ms}	=	main stage velocity
C_d	=	drag coefficient
m_t	=	total mass
g	=	gravity
ρ	=	air density
C_s	=	safety factor
A	=	area
A_{main}	=	area of main parachute
A_{drogue}	=	area of drogue parachute
f	=	safety margin
σ	=	allowable yield stress of the material
t	=	avionics thickness
P	=	pressure
d	=	average diameter
Fp	=	strength weight
SWR	=	standing Wave Ratio
h_{alt}	=	altitude

[1] Undergraduate Student, FEN/MECAN, igorsatopengmec@gmail.com
[2] Undergraduate Student, FEN/MECAN, fferreiragiulia@gmail.com
[3] Undergraduate Student, FEN/ELE, renanlarrieu@gmail.com.
[4] Undergraduate Student, FEN/MECAN, mylenaaapimentel@gmail.com
[5] Undergraduate Student, FEN/MECAN, marcusalves740@gmail.com
[6] Undergraduate Student, FEN/MECAN, rod_matheus2012@hotmail.com
[7] Undergraduate Student, FEN/MECAN, igorfelipe201615@gmail.com
[8] Undergraduate Student, FEN/MECAN, lucas.castro.fraga@gmail.com
[9] Undergraduate Student, FEN/DESC, ljunqueiracarneiro@gmail.com
[10] Undergraduate Student, FEN/ELE, caiomgb2@gmail.com
[11] Undergraduate Student, FEN/ELE, gabrielmaximus80@gmail.com

II. Introduction

Grupo de Foguetes do Rio de Janeiro (GFRJ) is a student-run organization of *Rio de Janeiro State University* (UERJ) dedicated to developing the aerospace science in the state of Rio de Janeiro through the development of our members' technical and professionally, by doing projects and science events all over the state. Every GFRJ's member can earn lots of knowledge and experience for a lifetime, either by participating in the management team or in the technical team. The main mission of the group is related to scientific education, trying a simple and enthusiastic approach on rockets, astronomy and space related content, working together with OBA (*Brazilian Astronomy and Astrophysics Olympics*) on events and workshops, to basic and high school students. This is a way the group found to contribute to the university, to science, and to the society at large.

The rocket team was founded in 2016 and it is the oldest group of the state, that is why the name makes a reference to the Rio de Janeiro. The GFRJ has a large historic of rockets and motors of your own authorship, which was only possible because the UERJ community always supported the group, either for academic support or the money donated from the students and teachers. Besides the financial help of the general people of the university, the team counts on the sponsorships of companies who want to contribute to science and the development of the members of the group.

Our team is organized by the following organizational chart, as can be seen in Fig. 1.

Fig. 1 GFRJ's organizational chart.

The rocket team decided to organize itself that way because of the new strategic planning. The Objective and Key Results (OKR) was adopted as a form to accomplish every goal planned by the directory.

The management team is responsible to earn and manage the resources of the group. The main idea is making GFRJ have exponential results with its own forces and for that it counts on a Management Director and 3 managers: Financial, Marketing and Human Resources.

The project team is responsible to study, plan and execute everything related to the maintenance and development of the rockets for the competitions and events. For that it counts on a Project Director and 6 managers: Recovery, Propulsion, Aerodynamics, Structures, Avionics and Payload.

The President is responsible to represent GFRJ's meanings inside and outside the group and to make the action plan works integrated with all team.

The GFRJ has its organization on 3 levels: strategic, tactical and operational. On the strategic level, the directory has the role to decide the objectives to be fulfilled and think all the action plan, considering only the goals wanted by the group. The tactical level is formed by the managers, and they are responsible to lead the operational level to realize every action in the action plan. The operational level is responsible to execute every action demanded by the managers. Worth mentioning that this is the way of strategy that every action is planned to achieve the goals thought by the directory.

III. System Architecture Overview

ATOM III is a 3100 mm length, 118 mm diameter launch vehicle designed to reach 3km AGL, divided into three modules and equipped with a solid propelled student-built motor, a recovery system by CO_2 ejection systems, a 3-ring mechanism, one COTS and one student-developed embedded system. The rocket will carry a Payload with a biological experiment. Furthermore, the flight stages can be analyzed in Fig. 2 and ATOM III design in Fig. 3.

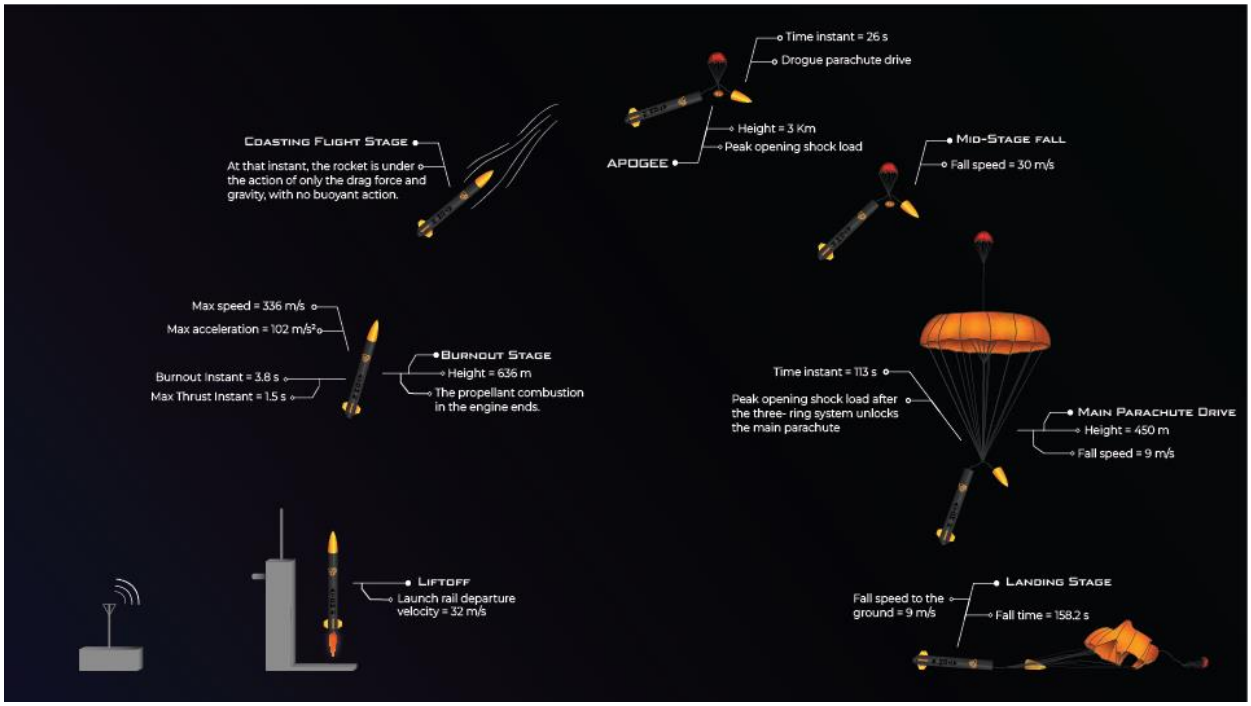

Fig. 2 *ATOM III* Flight Stage.

Fig. 3 *ATOM III*.

A. Propulsion Subsystems

The *ATOM III* rocket engine is called the MXT and uses a solid propulsion system. The MXT is designed in a simple and robust way with the objective of minimizing the number of parts in its construction to allow greater practicality in its assembly and manufacture. The engine in the exploded view is represented in Fig. 4 and each of its components are mentioned and described as:

- *Combustion chamber*: Component that contains the propellant and where ignition takes place.
- *Nozzle*: Component through which the gases from the burning of the propellant are drained from the combustion chamber.
- *Bulkhead*: Acts as sealing off one end of the rocket engine.
- *O-rings*: They are positioned in small gaps located in the nozzle and in the bulkhead so that the seal is guaranteed in the system.
- *Screws*: Components for attaching the nozzle and bulkhead to the combustion chamber.
- *Propellant Grain*: Acts as the fuel for the rocket to start its trajectory.
- *Inhibitors*: Wrap the propellant grains individually to inhibit burning.
- *Thermal protection*: It is used between inhibitors and the combustion chamber, absorbing part of the thermal energy from propellant burning.

Fig. 4 Exploded view of the MXT engine

1) The propellant

The MXT engine uses potassium nitrate (KNO_3) as an oxidant and sorbitol ($C_6H_{14}O_6$) as a fuel as solid propellant. The cited mixture is also referred to as KNSB.

The choice of KNSB as the composition of the solid propellant was due to its ease of manufacture combined with the curing time being long enough for the molding procedures to be successful. Furthermore, the performance generated by the KNSB is satisfactory for the purpose of the projected rocket.

Using *RPA* and with an oxidizer/fuel ratio of 1.883, KNSB has the ideal properties as shown in Table 1.

Table 1 KNSB's ideal characteristics

Molecular Weight (g/mol)	182.2
Melting Point (°C)	110
Density (g/cm^3)	1.84
Enthalpy of Formation (kJ/mol)	-1,353.7

To ensure the quality of the material used to compose the propellant used in the MXT engine, burn rate tests were performed as shown in Fig. 5, thus obtaining values that approach the theoretical values.

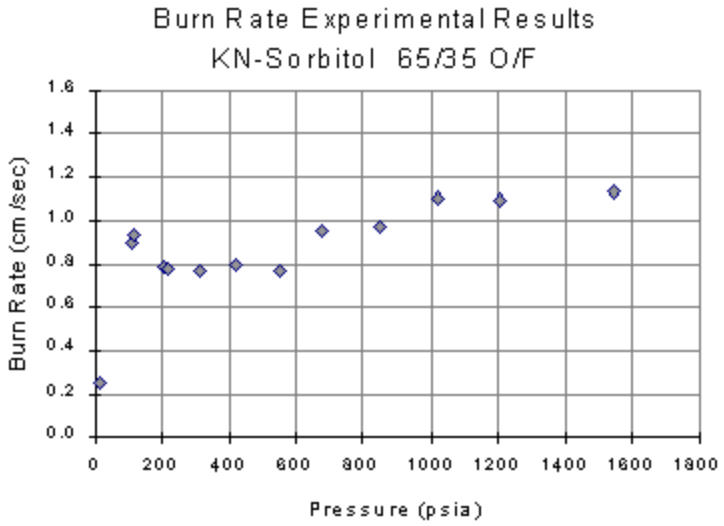

Fig. 5 KNSB burn rate experimental results.

2) Sizing and Theoretical Data

The solid propulsion MXT engine consists of an arrangement of bulkhead, casing, nozzle, propellant grain and inhibitors as shown in Fig. 6.

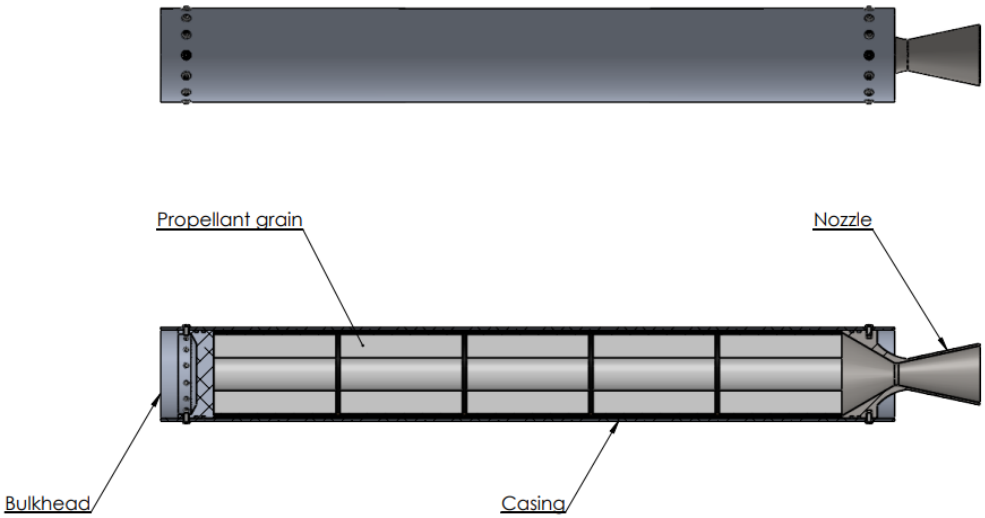

Fig. 6 Arrangement of MXT engine components.

The combustion chamber of the MXT engine is composed of a 6063-T5 aluminum alloy cylinder whose internal diameter measures 107.95 mm. Its available length for the accommodation of the propellant segment is 770.5 mm, resulting in an available internal volume of 6.28 x 10^{-3} m³, or 6.28 liters.

The nozzle present in the engine structure was machined from a 316 stainless steel billet, obtaining a diameter in the throat region of 27 mm, a half-angle of 30° in the convergent region and a half-angle of 12° in the divergent region.

The propellant used is composed of potassium nitrate with sorbitol in the proportion of 4.95 kg and 2.67 kg, respectively. In addition, the geometry used in the propellant grain follows the BATES geometry, with five axially rowed segments, each with an inhibitor made of paper 40 kg. The propellant grain is illustrated according to Fig. 7 and its dimensions, as well as some other additional information, are referenced in Table 1**.** Protecting the casing from the thermal loads, a thermal protection made by ethylene-propylene-diene monomer rubber (EPDM) is used.

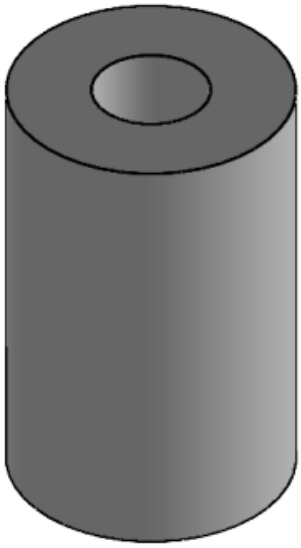

Fig. 7 Unit propellant grain.

Table 2 Propellant design data

Length [mm]	150
Diameter[mm]	97
Core diameter [mm]	40
Number of segments	5
Total Weight [kg]	7.62
Density [g/cm³]	1.65

The engine developed in the project uses the concept of student research and developed (SRAD) and is classified as an M-class engine, being able to deliver a total thrust of 9,384.4 N·s. The thrust-time graph is shown in Fig. 8 and Table 3 lists the data obtained from this graph.

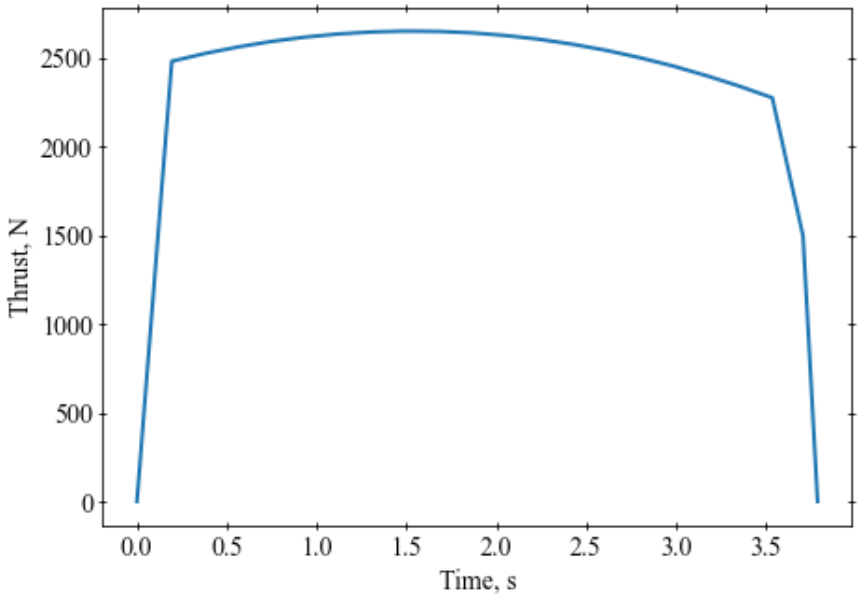

Fig. 8 Thrust-time graph developed by the MXT rocket engine.

Table 3 Final theoretical data

Average Thrust [N]	2,489.08
Maximum Thrust [N]	2,651.42
Total Thrust [N]	9,392.51
Specific Thrust [N]	125.67
Maximum Pressure [psi]	500

Later, in the Annex of the Test Report, the experimental data of the MXT collected in the Fire Test can be viewed, along with its comparison with theoretical data.

3) Structure

After the theoretical dimensioning of the loads acting on the motor, the construction aspects of the project are defined. As mentioned before, the material chosen for the engine was aluminum alloy 6063-T5 due to its ability to withstand the exposed operating conditions, making use of the thin-walled pressure vessel equation considering a cylindrical vessel, as is the case of the engine used in the project. This equation is expressed according to Eq. (1).

$$f = \frac{2\,\sigma\,t}{P\,d} \tag{1}$$

Using the theoretical yield strength of 6063-T5 aluminum alloy of 105 MPa and a combustion chamber thickness of 3.175 mm, a design safety margin equivalent to 1.79 is obtained.

To fix the nozzle and bulkhead in the combustion chamber, 28 screws are positioned with a resistance class of 12.9 in total, 14 of them at the end where the bulkhead is positioned, and the other 14 screws present at the end where the nozzle is positioned.

B. Structure Subsystems

The structural design of the *Atom III* was developed following the purpose of obtaining an airframe with good mechanical properties and low specific mass. Due to that, the fiber glass-epoxy resin composite was selected, in which the epoxy resin acts as the polymeric matrix capable of evenly distributing the loads acting on the glass fibers arranged under +0/+90 orientation.

The fiberglass-epoxy resin composite guarantees important characteristics in the project, such as high mechanical resistance to traction and compression and excellent resilience in case the rocket body is required to protect the internal components most vulnerable to impacts from falls from large altitudes, in addition to the low specific mass of the material that allows a better use of the apogee reached by the rocket.

In order to improve the structural finish and reduce the drag coefficient, a layer of gel coat was applied throughout the outside of the rocket.

1) Nose cone

The nose of the *Atom III* rocket follows the LD-Haack design, also known as the *Vón Kármán* nose. This selection was preferred due to the fact that this nose is able to reduce the efforts from the drag force that causes considerable loss in the apogee of the project to be reached by the rocket. With this, the *Vón Kármán* will act by reducing the drag coefficient of the rocket in the subsonic/transonic flight region.

In making the *Vón Kármán*, we chose to use the 3D printing manufacturing process in most part of the structure, which allows the project the possibility of obtaining precise measurements and of easy production. The material used in the 3D printing of the nose is ABS. The hood nozzle will be manufactured using subtractive manufacturing, where, using a CNC lathe, it will be machined with the proper parameters. The material used in the machining was 6153-T6 aluminum. The design can be seen in the Fig. 10.

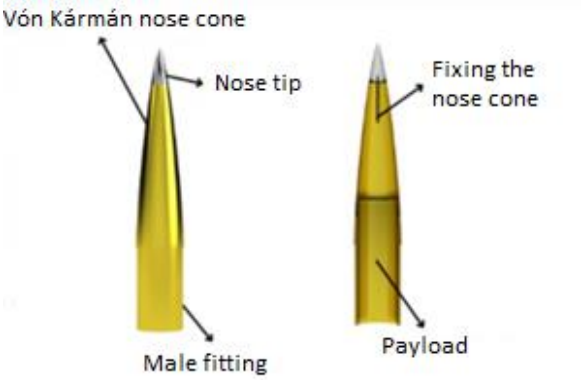

Fig. 9 *ATOM III*'s nose cone

2) Couplers

The couplers play a fundamental role in the structure of the *Atom III*. They have the function of joining the modules together in a stable way and also act to protect and secure the parachute ejection system. In addition, it is designed to meet the need to allow communication between avionics and recovery systems. The design can be seen in Fig. 11.

The material used in the couplers is 6351-T6 aluminum alloy, which meets the requirements of mechanical strength and also due to its reduced specific mass compared to steel. In addition, this alloy is easy to machine, which allows it to be easily produced.

Considering that the recovery system will be through the use of gas, it was necessary to adapt the couplers. Aiming at good impermeability, pairs of o-rings and parbaks will be used.

For fixing the parts of the couplers, a 3mm nylon thread will be used. The nylon thread will fill a cavity, as can be seen in Fig. 12 which will make it impossible to uncouple them during the flight. The couplers will be fixed to the fuselage by Button Head Socket Screw.

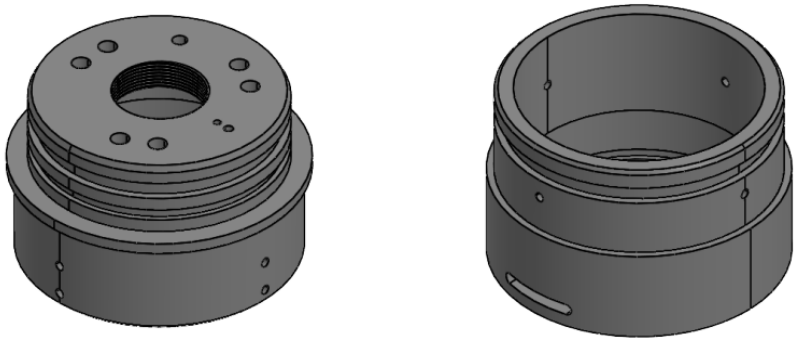

Fig. 10 *ATOM III* Couplers

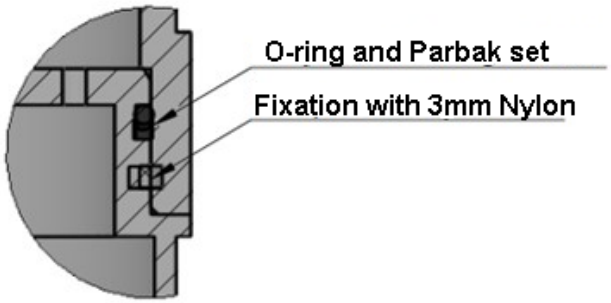

Fig. 11 *ATOM III* Fixation Couplers

C. Aerodynamics Subsystems

Flight and performance simulations were performed in the *OpenRocket* software. The rocket's first design in Fig. 12 was developed by the program, estimating masses and measurements of the components. Regarding the latest version (*ATOM II*), project updates were made to improve flight performance through mass reduction, such as diameter reduction, fin shape and boat tail implementation.

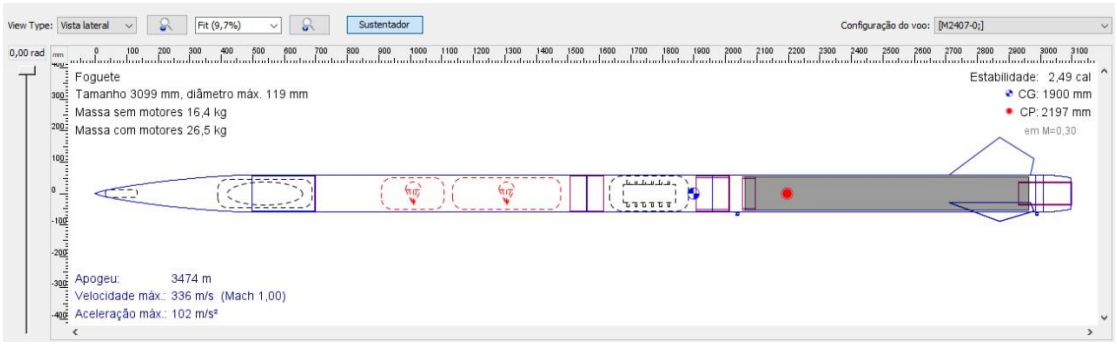

Fig. 12 *ATOM III* in *OpenRocket*.

1) Fins

The fins in Fig. 14 have their own design that meets the necessary stability criteria. These have sufficient area to bring the center of pressure down from the center of gravity at least 2.1 calibers, which meets the stability criterion throughout the flight.

A flutter analysis was performed using the NACA TN 4197 V2 method – Flutter Analysis. Flutter speed found with 50% safety factor was 337.41 m/s or approximately Mach 1.0. Higher speed than the maximum speed of the rocket during its flight.

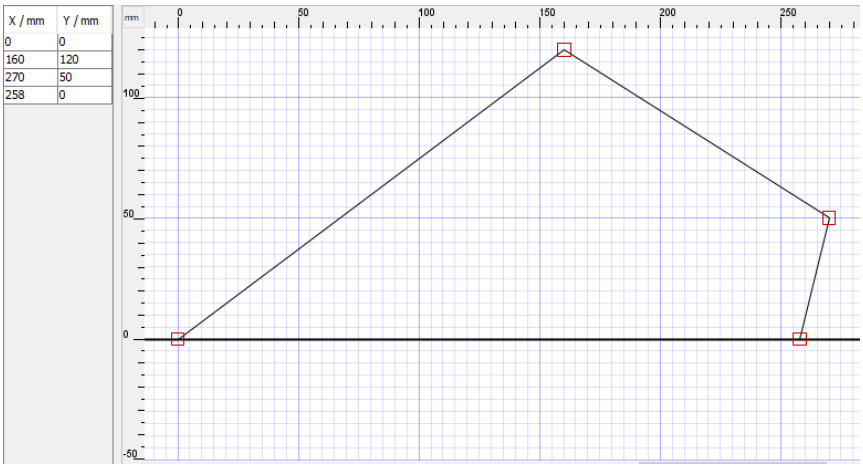

Fig. 13 Fins Dimensions.

2) Boat Tail

The implementation of the boat tail aims to reduce the base drag produced by the difference in diameter in the wind flow at the bottom. Due to that, its design was made from the Vón Kármán format, which was cut in the measure and desired diameters to offer the best performance.

3) Simulations

The *Atom III* presents a flight simulated profile through the software *OpenRocket* in Fig. 14. In this graph, data such as maximum speed and maximum acceleration achieved during the flight path can be extracted.

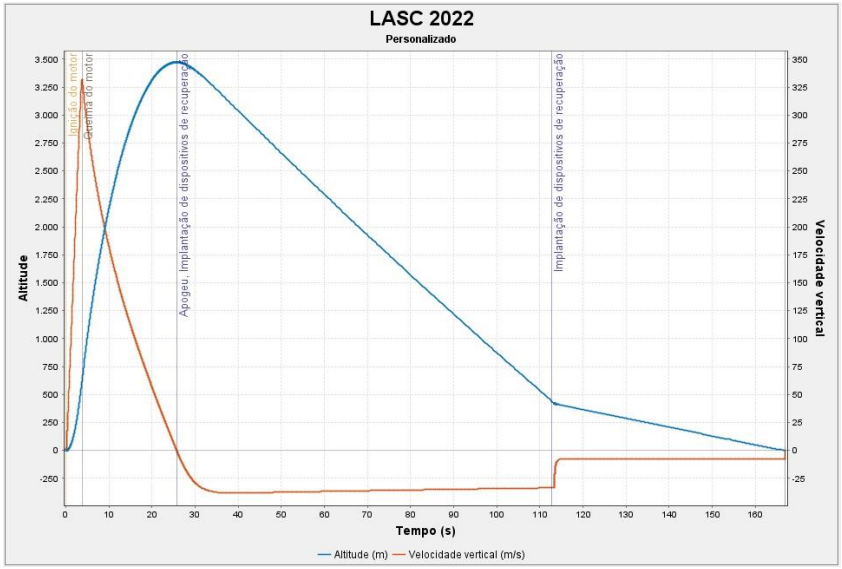

Fig. 14 Flight Simulation Profile.

The data collected through the all-important simulation are listed in Table 4.

Table 4 Flight Data

Maximum speed	336 m/s

Maximum acceleration	8.5 G

The predicted altitude reached by the *Atom III* is related to the time during its flight trajectory. Using the simulation performed by the *OpenRocket*, it was possible to reach a maximum apogee of 2780 meters, considering a target apogee of 3000 m. The graph represented in Fig. 15 expresses how altitude relates to time.

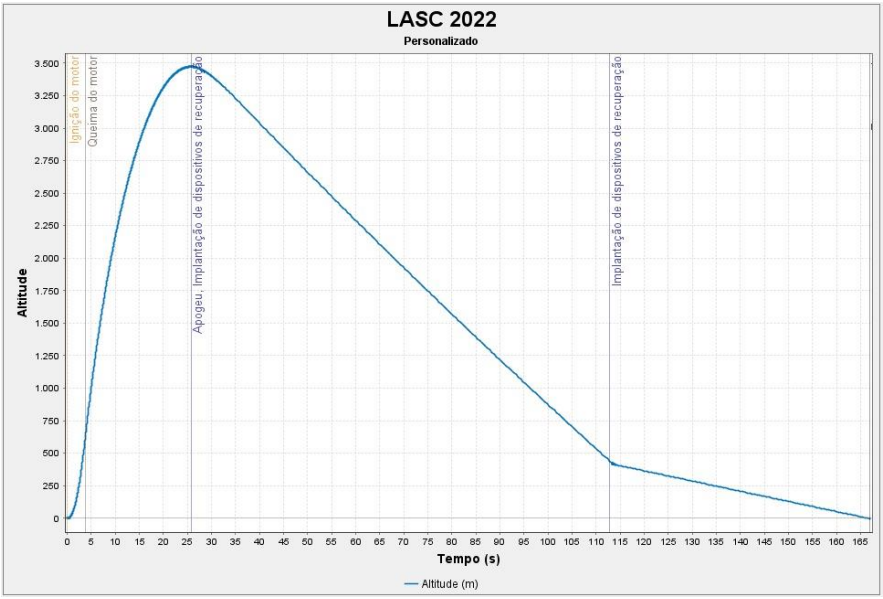

Fig. 15 Predicted altitude.

All simulations regarding aerodynamics considered the estimated weight of the rocket, including the fact that the rocket's mass varies with time during the flight path. The Table 5 lists the masses of some important segments.

Table 5 Component Masses

Vehicle weight	14.5 kg
Propellant weight (all)	8.0 kg
Payload weight	4.0 kg
Total liftoff weight	**26.5 kg**

In terms of aerodynamics, the centers of pressure and gravity are fundamental features in the design of the rocket. With them, the rocket can perform a stable and safer flight. Then, two simulation situations were considered to obtain these two points: static and dynamic.

The static simulation consists of determining the centers of pressure and gravity considering the rocket not being in motion. In this case, the positions of the centers of pressure and of gravity are listed in the Table 7. Essentially, considering this case, the minimum static margin during the thrust is 2.

Table 6 Position of the centers of pressure and gravity in the static simulation

Center of pressure	2197 mm
Center of gravity	1900 mm

In the dynamic simulation, the determination of the centers of pressure and of gravity varies over time, as the thruster system is consumed during the trajectory of flight. Thus, it is not possible to estimate a fixed value for both.

However, it is possible to estimate values for each time interval through a graph produced through a simulation in the *OpenRocke*t as shown in the Fig. 17.

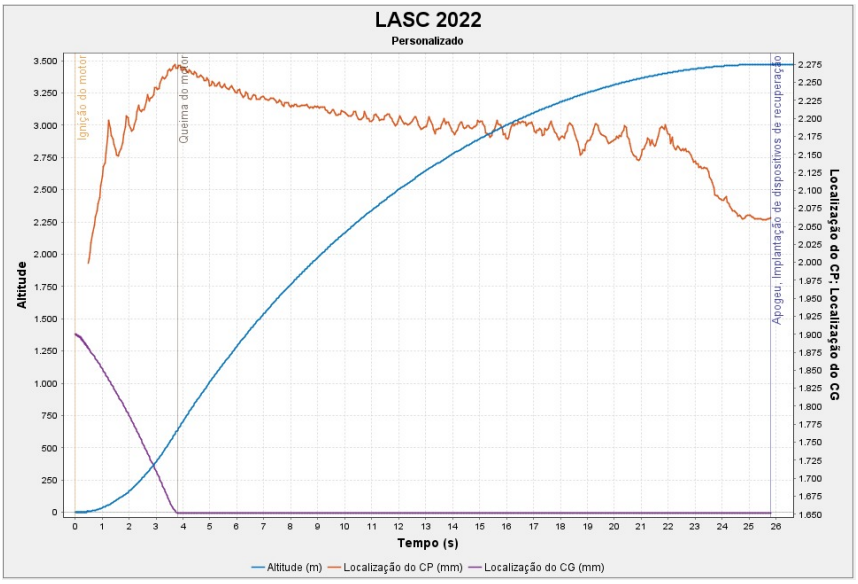

Fig. 16 Simulated center of pressure and simulated center of gravity.

D. Avionics Subsystems

The student-developed embedded system that compose avionics system is based on data acquisition, data telemetry and parachute drive. Essentially, the data acquisition subsystem acquires all the quantities listed in Table 7. Moreover, note that Altitude and Velocity are calculated variables rather than measured variables like the others. This is because the RRC3 Module calculates these variables from the pressure, which is also acquired by the GY-87 module, according to the Table 7.

Table 7 Avionics modules

Quantity	Module	Sensor
Atmosferic Pressure	RRC3/GY-87	MSI MS5607/BMP180
Altitude	RRC3	Calculated by Conversion
Velocity	RRC3	Calculated by Conversion
3-axis Position	GY-87	MPU-6050
3-axis Acceleration	GY-87	MPU-6050
3-axis Magnectic Field	GY-87	HMC5883L
Temperature	RRC3/GY-87	MSI MS5607/BMP180
Latitude	GPS NEO-M8	u-blox M8 GNSS
Longitude	GPS NEO-M8	u-blox M8 GNSS

The COTS altimeter that is used in avionics system, as mentioned before, is the RRC3 “Sport” Altimeter as the Fig. 17 shows. This device has a high reliability of operation, and for that reason it was selected by the team.

Fig. 17 COTS Altimeter RRC3

The device has in its core a 16-bit 16MHz Microcontroller, and it also has an 8Mbit SST Flash Memory to save all the data acquired during the flight. Furthermore, it has dimensions of 23.5 mm x 99.5 mm and the device is capable of delivering 3 A of current for 1 second during the trigger stage, which occurs twice – in the apogee stage and in the main parachute drive stage.

According to RRC3 manual, the RRC3 Module and the mDACS software both employ the NOAA "Pressure Altitude" calculation method to convert air pressure to an equivalent altitude. The conversion quoted in the Table 7 is calculated using the Eq. (2) to obtain altitude.

$$h_{alt} = \left(1 - \left(\frac{P_{sta}}{1013.25}\right)^{0.190284}\right) \cdot 145366.45 \tag{1}$$

The velocity of the vehicle can be calculated point by point by using the Eq. (3)

$$v = \frac{\Delta h_{alt}}{\Delta t} \tag{2}$$

The GY-87 module is connected to the ESP TTGO T-BEAN V1.1 on a printed circuit board – that can be seen in Fig. 18 - designed by the team, as is the SD module, which is responsible for recording all data acquired by the avionics system. But also, all data is sent to the base by the telemetry system, composed of a radio link established by the LoRa protocol, which was selected for its low consumption.

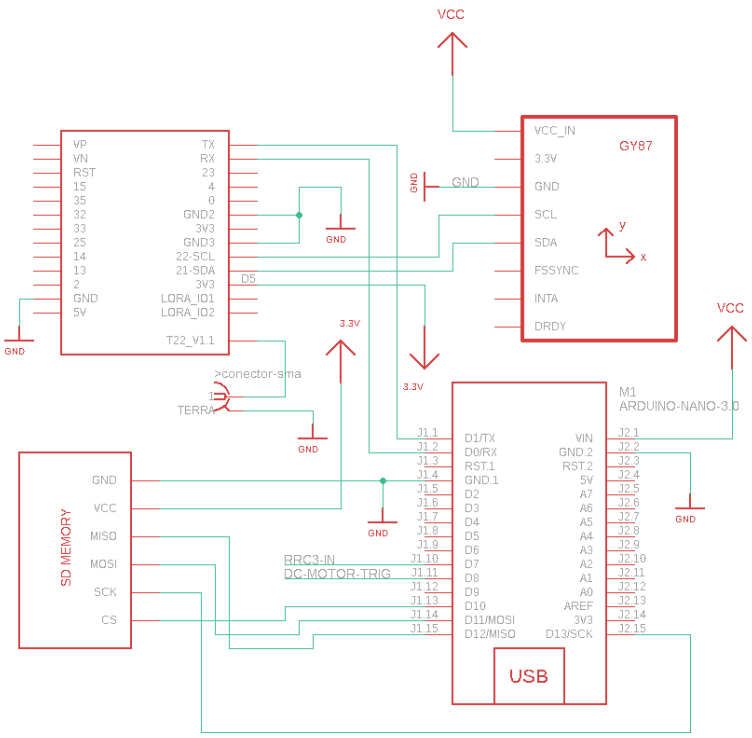

Fig. 18 PCB Scheme

The communication is enabled at the moment the system is powered on by removing the RBF from the rocket switch inside the avionics casing before the liftoff stage, which can be seen in Fig. 2. At this point, the communication is enabled and the antenna - disposed on the left of the drawing showed in Fig. 2 - starts to operate. This antenna. - which is shown in Fig. 20 - was designed to operate at its best gain in 433.775MHz, as can be seen in Fig. 19.

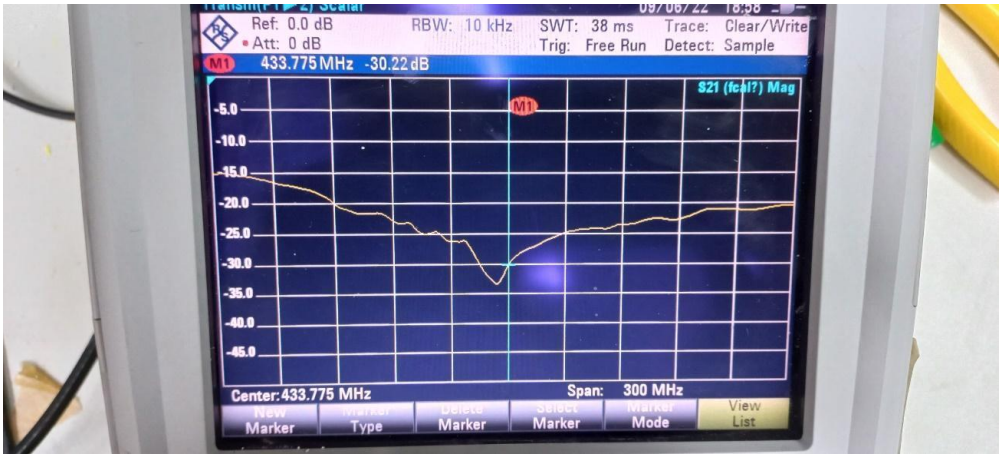

Fig. 19 Spectrum Analysis of the base antenna

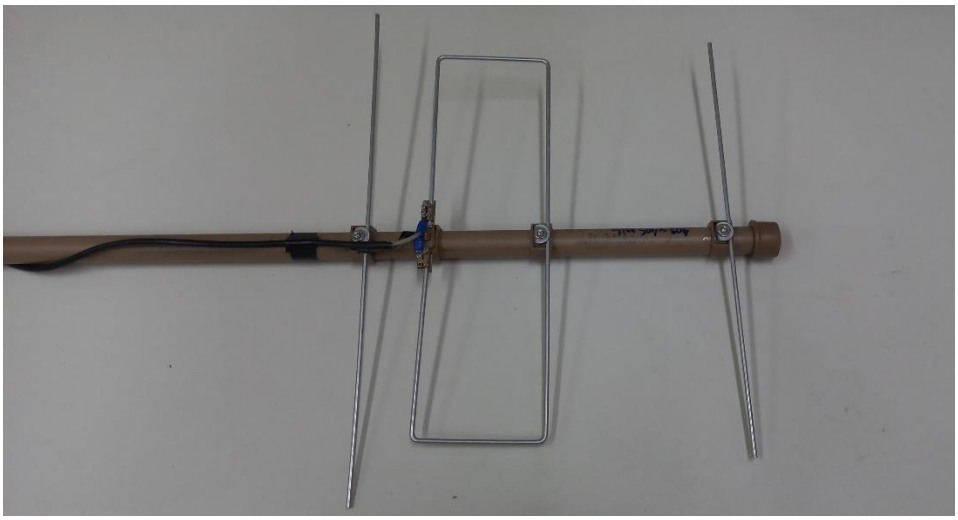

Fig. 20 Designed base antenna

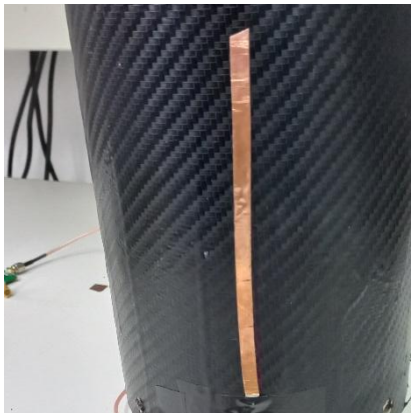

Fig. 21 Microstrip antenna

The *ATOM III* flight scheme that relates the angle between the antenna and the rocket position is described in Fig. 22. Note that the angles explicated in the figure are related to three defined altitudes, assigned from 1-3.

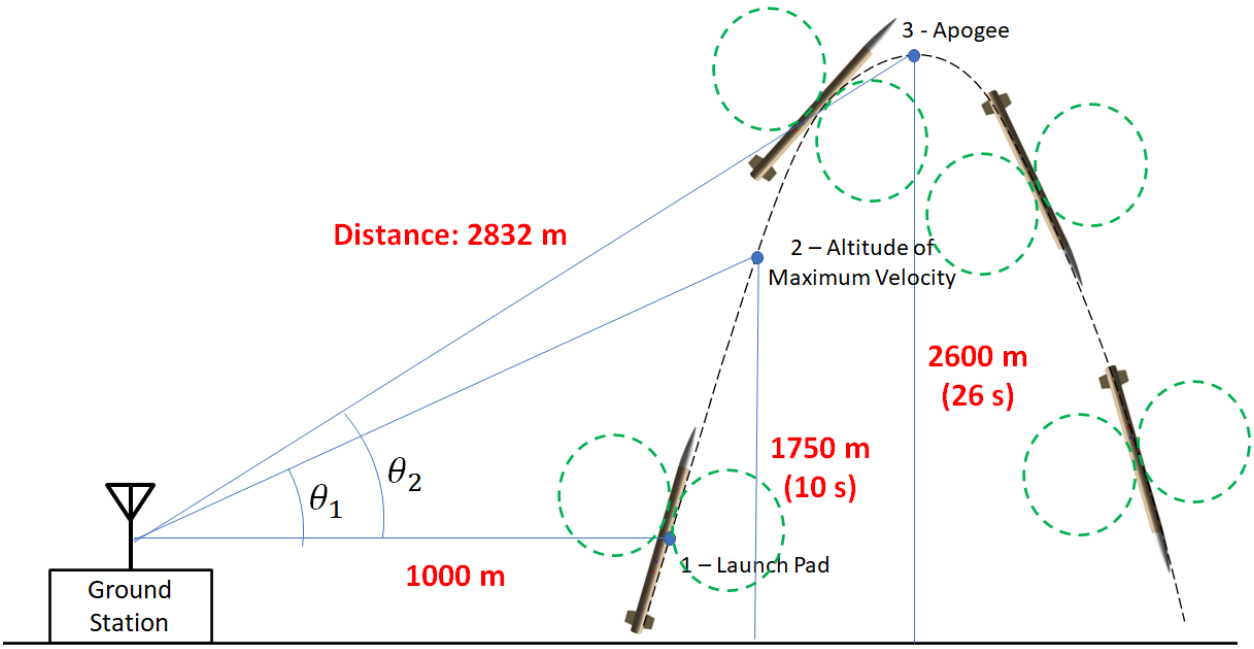

Fig. 22 Telemetry scheme

Therefore, analyzing Fig. 22, it is noted that θ_1 and θ_2 can be calculated, as well as their variations in time.

$$\theta_1 = \arctan\left(\frac{1750}{1000}\right) = 60° \tag{3}$$

Also,

$$\dot{\theta_1} = 6°/s \tag{4}$$

Similarly,

$$\theta_2 = \arctan\left(\frac{2600}{1000}\right) = 69° \tag{5}$$

$$\dot{\theta_2} = 2.6°/s \tag{6}$$

In terms of telemetry, initially was considered to use just a unit of copper strip to the microstrip antenna, disposed on the surface of the rocket, like shown in the Fig. 23. Assuming that configuration in simulations, we could conclude that the radiation pattern on that case is very asymmetrical and non-uniform during the rocket rolling, as can be seen in fig below. In addition to that, it can be exposed that in this configuration we have a lower gain and a $SWR = 2.52$.

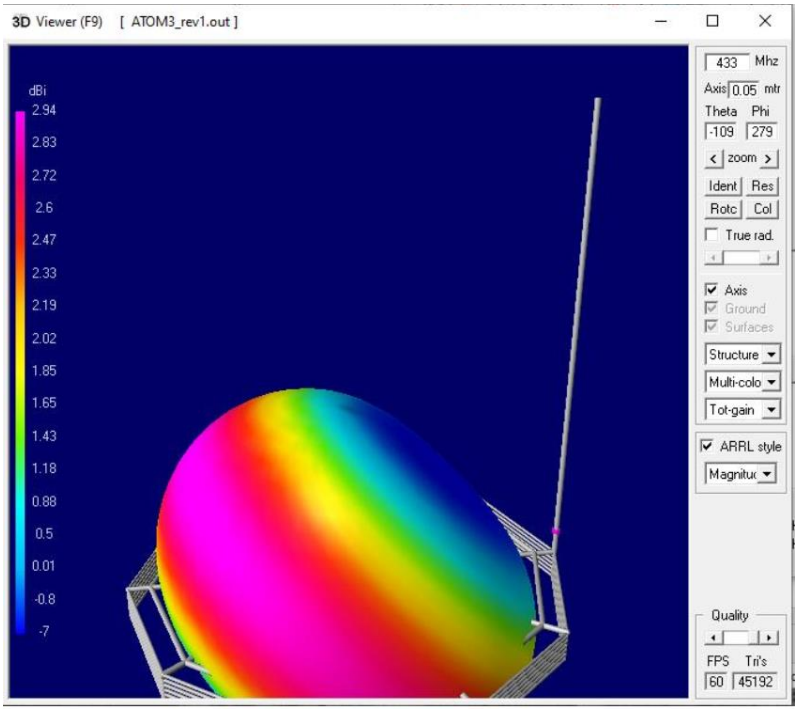

Fig. 23 Single copper strip simulation

On the other hand, considering two units of copper wire for the microstrip antenna, arranged side by side on the surface of the rocket we obtained better simulation results, as Fig. 24 shows. This fact implies that this arrangement fits better to operate on the *ATOM III*.

On that configuration, was obtained a more symmetrical and uniform radiation pattern, a better gain and a $SWR = 1.05$.

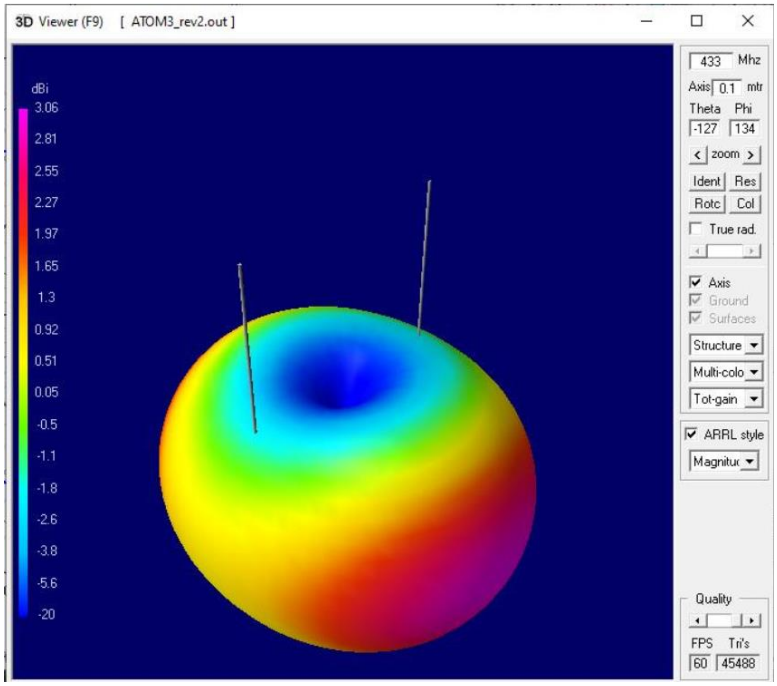

Fig. 24 Dual copper strip simulation

Thus, considering the last configuration, we obtained the gain as follows in Table 8:

Table 8 Antenna Gain for each α

α	Antenna Gain
10°	−12.4 dBi
20°	−6.49 dBi
30°	−3.15 dBi
40°	−0.91 dBi
50°	−0.67 dBi
60°	+1.78 dBi
70°	+2.52 dBi
80°	+2.94 dBi
90°	+3.06 dBi

The gain values shown in the table above, in terms of α describe the following antenna gain curve, which is the total gain in the 2D vertical plane, as can be seen in .

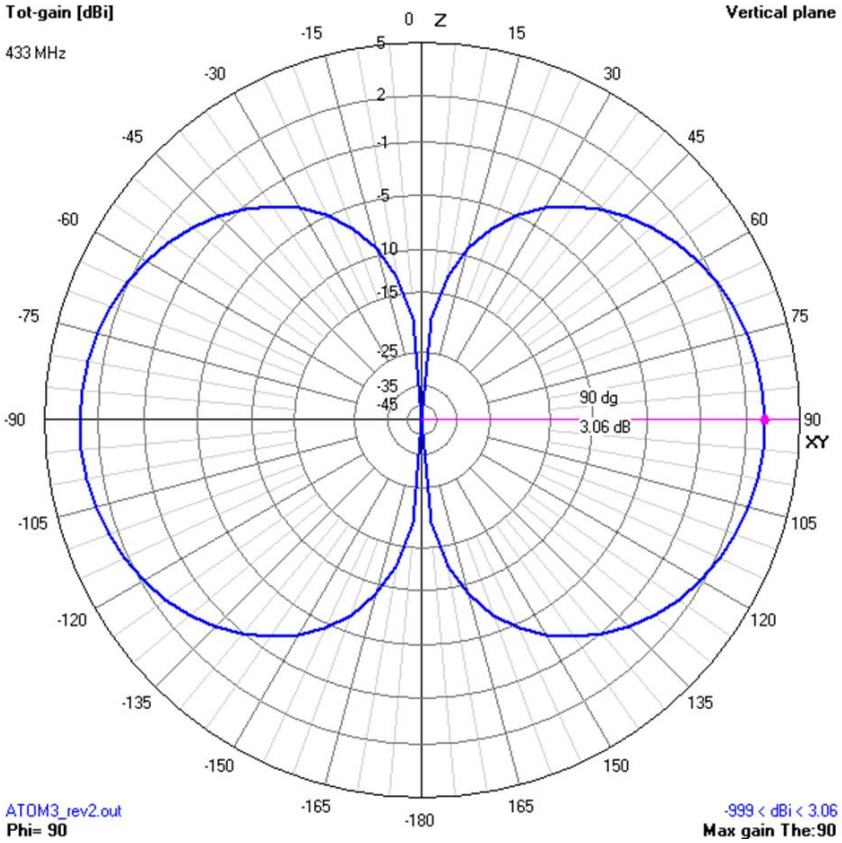

Fig. 25 Vertical plane 2D radiation pattern.

Also, it can be seen the total gain in 2D horizontal plane in Fig. 26.

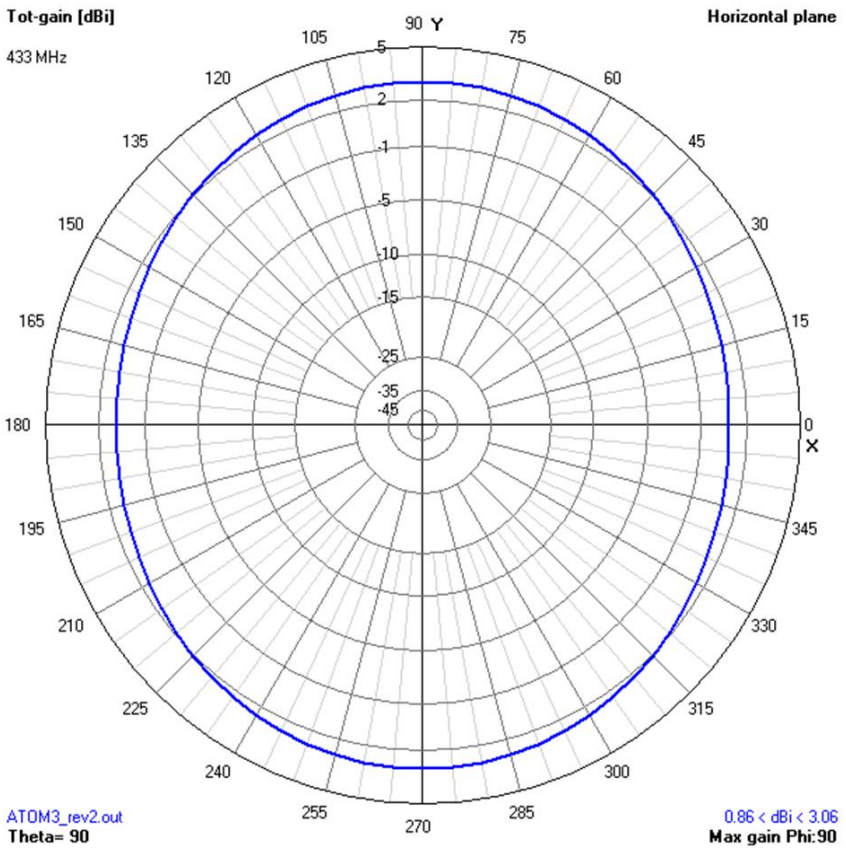

Fig. 26 Horizontal plane 2D radiation pattern.

Considering the antenna with two copper strips, and the diagram described in the figure below, the analysis of the losses of the link between the base station and the rocket is carried out.

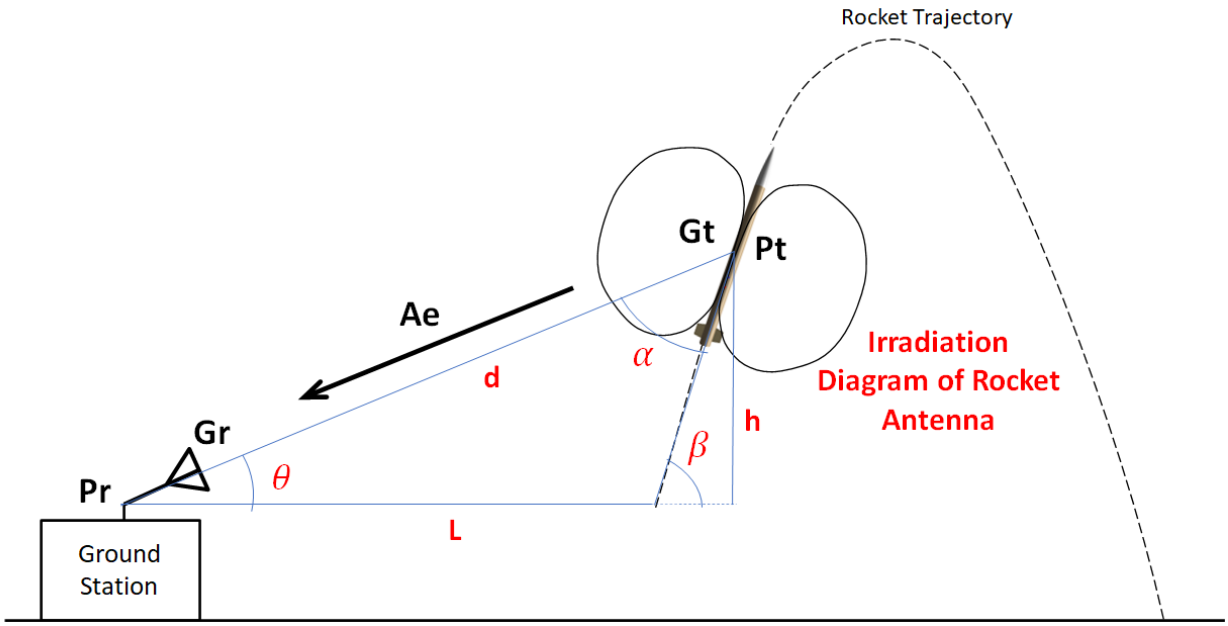

Fig. 27 Telemetry scheme.

Thus, losses can be calculated from Eq. (7).

$$\Pr(dB) = Pt(dBm) + Gt(dB) + Ae(dB) + Gr(dB) \quad (7)$$

Pt – Output power of the transmitter on the rocket
Gt – Gain of the rocket antenna (function of angle α)
Ae – Attenuation of the link (a function of the distance d, and the frequency)
Gt – Ground antenna gain
Pt – Power at the receiver input

E) Recovery Subsystems

The recovery system of the *ATOM III* rocket will be triggered two times during the flight, as shown in Fig. 2. The system consists of 2 parachutes - the first one with a smaller area and the second one with a larger area, called drag and main parachutes respectively - 2 CO_2 ejection systems, a 3-ring mechanism, a gunpowder container for redundancy and a thermal protection blanket. The CO_2 ejection unit can be seen in Fig. 28, and its exploded view, in Fig. 29. In addition to that, it can also be seen the full CO_2 ejection system in Fig. 32.

The first event occurs when the vehicle reaches its apogee, so a drogue parachute is ejected and the vehicle experiences slowdown. This ejection is triggered by the COTS altimeter, which identifies the apogee altitude and sends an electric signal to the recovery system. At this time, the gunpowder located inboard at the bottom of the CO_2 ejection unit in Fig. 28 is ignited and the piston moves up. This described movement creates enough pressure to the side outputs and then it ejects the drogue parachute, breaking the rocket on the nose cone, which sorts out the vehicle in two parts. After that, the vehicle is expected to be at a constant speed of 30m/s with the three-ring system locking the main parachute, exactly as illustrated in Fig. 30, until the 450m of altitude.

At this altitude, the COTS altimeter sends an electric signal that drives a DC motor to pull a rope of the three-ring system, which unlocks the main parachute, as Fig. 31 shows. After that, the vehicle experiences a great peak opening shock load, and it starts to be slowed down at a constant speed of 9m/s until the gentle land.

The dimensions of the CO_2 cylinder and the parachute system can be seen respectively on Fig. 33 and Fig. 34.

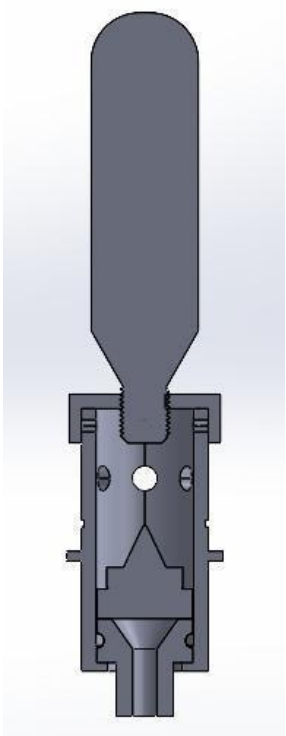

Fig. 28 CO2 Ejection Unit.

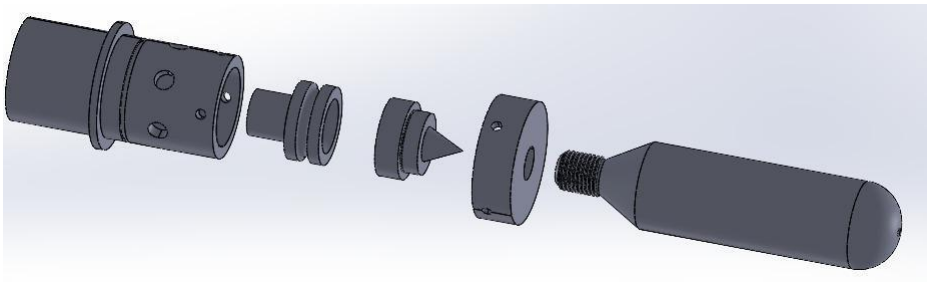

Fig. 29 CO2 ejection unit exploded view.

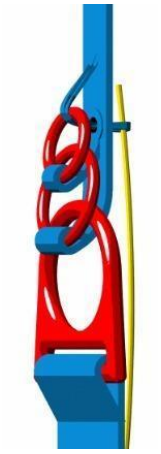

Fig. 30 Locking stage three ring system.

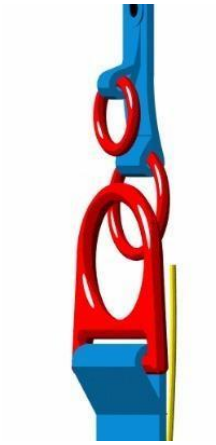

Fig. 31 Unlocking stage three ring system.

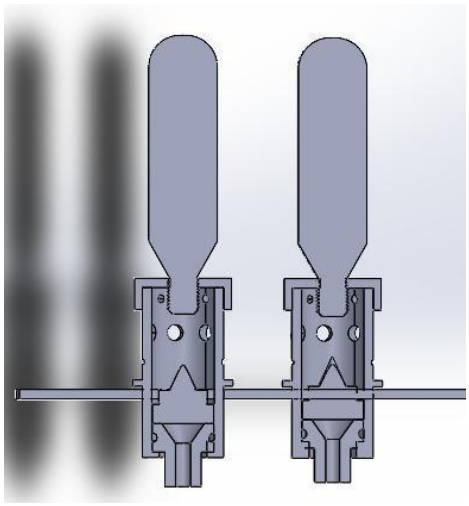

Fig. 32 CO2 complete system.

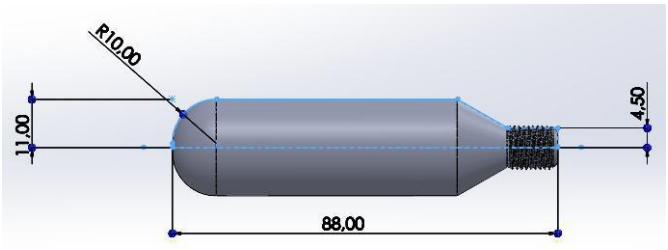

Fig. 33 CO2 Cylinder dimensions.

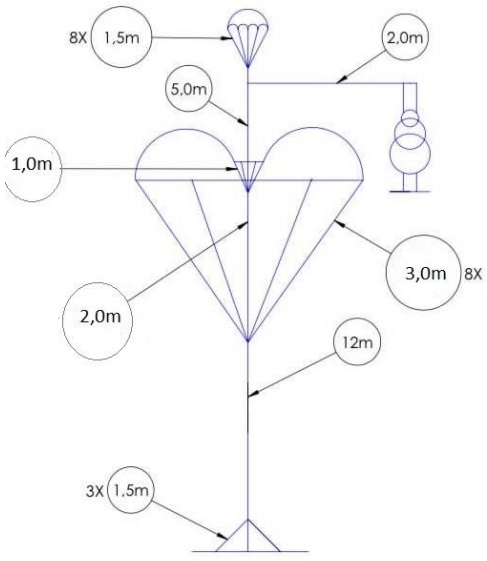

Fig. 34 Parachute system dimensions.

Subsystem Components

1) Drag parachute

The drag parachute was produced by the team itself, using high-resistance nylon 044 ripstop fabric and has a circular geometry, in red with an area of 0.720 m². In addition, it has a spill hole with a diameter of 0.15 m. This parachute will be ejected at apogee, that is, when the speed is zero, then the force on the drag lines will be less than on the main one, which is ejected during the fall, so 8 suspension lines made of Kevlar will be used, each 1.424 m long. The trailing parachute is housed above the main one and has two anchors (1000lbs Kevlar cable), one on the main parachute and the other on the three-ring system, connected to the anchor ropes.

2) Main parachute

The main parachute was produced by the team itself, using the high-resistance Ripstop nylon 044 fabric, and has a semi-elliptical geometry, in orange color, with an area of approximately 3.23 m² distributed in 8 sections. In addition, it has a spill hole - a hole in the center of the parachute - with 0.32m in diameter to reduce oscillation during the fall. Thus, in this project there will be 8 suspension lines made of 300lb Kevlar, each 3 m long, and a central line that connects the center of the spill hole. Moreover, the parachute is housed just below the trailing parachute and will be ejected at a height of 450m, as explained before, and has a 3-point distributed anchor (44kgf/cm Kevlar tape) in the upper coupler.

3) CO_2 system

The ejection system that pressures the nose cone to be ejected are composed of 2 cylinders containing 24g of CO2, which will be broken by a needle piston, each one, which will be moved by an explosion of an exact amount of powder, which will be pressurized inside a compartment and will be activated. from a squib. The gas pressure will eject the nosecone releasing the drag parachute.

4) 3-ring system

The 3-ring system is responsible for preventing the drag parachute force from pulling the main parachute to the desired height. For this, the system designed consists of 3 rings that intertwine in 2 strips of kevlar, these rings held by a wire, when the rocket reaches 450m, a DC motor will pull this wire, releasing the drag parachute and thus pulling the main parachute.

Calculation of the Parachute Area

The main idea is to make the rocket land on the ground with constant known velocity. For this, it is necessary to make the vertical component of the Resultant Force F_R of the rocket equal to zero, as described on the Eq. (6). For then, the Rocket's Weight P, given by the Eq. (7) must be equal to the Drag Force F_a, given by the Eq. (8). Thus, we have Eq. (9) as result, followed by the Eq. (10) and the Eq. (11).

$$F_R = \sum_{i}^{\infty} F_i = 0 \tag{8}$$

$$P = mg \tag{9}$$

$$F_a = \frac{1}{2}\rho v^2 A C_d \tag{10}$$

$$P - F_a = 0 \tag{11}$$

$$P = F_a \tag{12}$$

$$mg = \frac{1}{2}\rho v^2 A C_d \tag{13}$$

Thus, the Eq. (12) is obtained

$$A = \frac{2mg}{C_d \rho v^2} \tag{14}$$

Therefore, considering

$$v_{ds} = 30\ m/s$$

$$v_{ms} = 9\ m/s$$

$$C_d = 1.4$$

$$m_t = 21.2\ kg$$

$$g = 9.80665\ m/s^2$$

$$\rho = 1.1062\ kg/m^3$$

$$C_s = 1.5$$

It is then calculated that the area of the main parachute is,

$$A_{main} = 3.23\ m^2 \tag{15}$$

And the drogue parachute,

$$A_{drogue} = 0.376\ m^2 \tag{16}$$

Also,

$$A_r = A_p = \frac{\pi d^2}{4} \tag{17}$$

$$d = \frac{\sqrt{4A_p}}{\pi} \tag{18}$$

Table 9 Fall Speed

Drogue Stage	30 m/s
Main Stage	9 m/s

F) Payload Subsystems

The Payload subsystem consists of a scientific experiment in which it aims to evaluate the maintenance of cell integrity of a species of unicellular photosynthetic microalgae, called *Chlorella vulgaris*, when subjected to an altitude of 3,000 m and to the efforts applied during a launch of rocket. In addition, it is also evaluated how such changes are impacting factors with regard to the production of bioproducts by the microalgae of study.

To accommodate the scientific experiment, the Payload is classified as a unitary CubeSat (1U), which have dimensions of 10 cm x 10 cm x 10 cm. In this configuration, carrying out the experimental procedure becomes feasible with good usability for research purposes.

1) Experimental bioassay

The photosynthetic unicellular microalgae Chlorella vulgaris is cultivated and maintained in an incubator with photoperiod and temperature control, as evidenced in the ABNT NBR 12648 Standard (ABNT, 2011). Such cultures are replicated at a monthly frequency and the growth and development of the cultures are monitored biweekly by manual counting in an optical microscope and by chlorophyll measurement in vivo by fluorescence (485 nm of excitation and 685 nm of emission).

Microalgae pre-culture starts five to seven days before the bioassay, the latter being revered as the launch day of the ATOM III, in L.C. Oligo medium, where they are in an exponential growth phase. Thus, on the day of the bioassay, the cultures are transferred to the analysis tubes and flasks and are manually shaken, starting the experimental procedure. For analysis purposes, the initial microalgae biomass on the day of the bioassay is 105 algae/mL.

The static bioassays of microalgae Chlorella vulgaris are performed to evaluate the effect of exposure to acceleration and vibration submitted by a rocket whose predicted apogee is 3,000 m with a colorimetric monitoring of the bioassay culture. In addition, the following are analyzed in microalgae: the degree of sedimentation; the degree of cell integrity; and the production of bioproducts of commercial interest. Fig. 35 shows the arrangement of microalgae on an analysis slide being observed under an optical microscope.

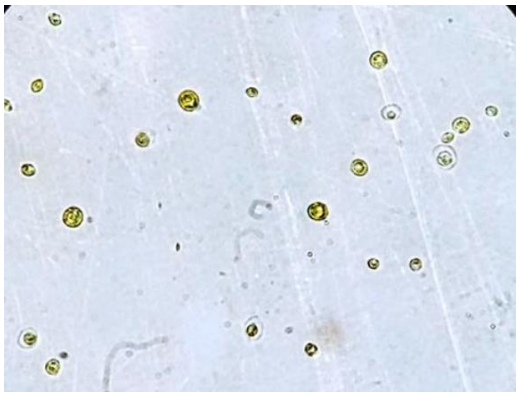

Fig. 35 Microalgae of the species Chlorella vulgaris under an optical microscope (400x).

The degree of microalgae sedimentation is determined using two different methods. The first one is followed by colorimetric measurement of the culture in a cell culture flask (on a flat surface) every 3 seconds and after the arrival

of the same in soil. Fig. 36 shows the type of vial used in the method in which the colorimeter is used in the measurement. In the second method, the analysis is determined from the visualization of the microalgae precipitate at the bottom of the Falcon tubes and from the determination of the value according to the scale present in the tube. Fig. 36b shows what the Falcon flask on which the second method is evaluated looks like.

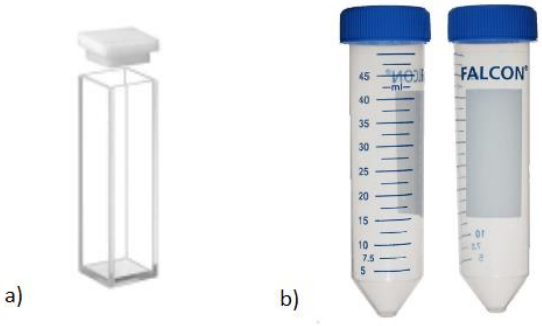

Fig. 36 (a) Culture flask and cells (flat surface); (b) Falcon tubes (cylindrical shape and conical bottom).

The results of both methods are compared with the results presented in the laboratory cultures during the same period. Such results will be statistically analyzed in statistical software in a post-launch period in specialized laboratories at the University of the State of Rio de Janeiro.

The degree of integrity of microalgae cells is determined by counting viable microalgae cells under an optical microscope with 400x magnification, in a Neubauer chamber, and preserving 1 mL of algal samples in lugol solution.

After the Payload is recovered, the Falcon tubes containing the microalgae cultures will be sent to the laboratory for analysis. The extraction of bioproducts of commercial interest is performed to characterize the microalgae biomass in relation to the content of proteins, carbohydrates, total lipids and fatty acids by gas chromatography in a GC-MS.

2) Electronic and structural assembly

In order to carry out the experimental procedure in terms of evaluating the maintenance and cellular integrity of the microalgae *Chlorella vulgaris*, a colorimeter is built whose optical sensor OPT101 acts as the main component, in which it measures the intensity of the absorbed light given a reddish color from LED lighting. With this, the microalgae sedimentation observed during the trajectory of the *ATOM III* is measured.

The electronic equipment used in the aforementioned scientific experiment are listed as: battery 9V, micro-SD card module, optical sensor OPT101 and LEDs.

Figure 1 show a schematic in which the presence of a resistor connected to two inputs on the OPT101 optical sensor is highlighted, as shown in Fig. 36 which represents the sensor block diagram. With the connection between such components established, a greater usability of the results during the bioassay is obtained.

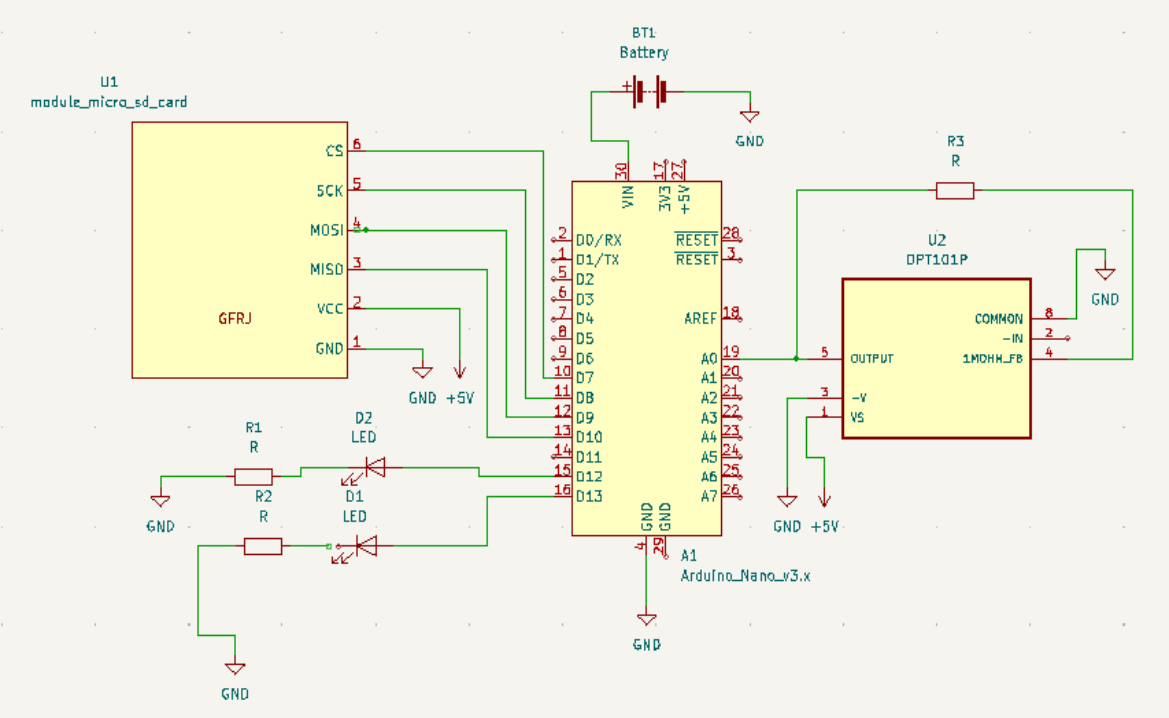

Fig. 37 Schematic representation of the Payload electronic system

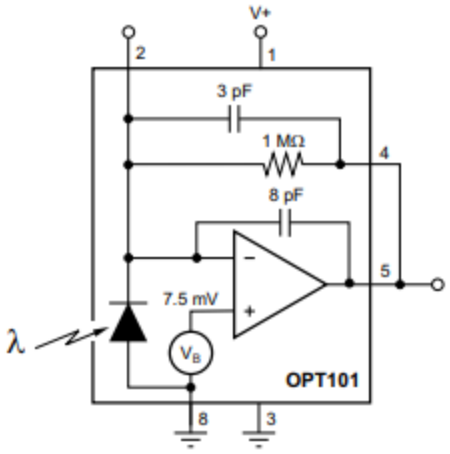

Fig. 38 OPT101 sensor block diagram

.

The physical structural representation of the OPT101 optical sensor is given by Fig. 36, a component that is present in the electronic arrangement of the scientific experiment.

Fig. 39 Physical structure of the OPT101 optical sensor.

The construction of the structure that holds the colorimeter was carried out through 3D printing, since this process allows greater practicality in generating complex geometries that can efficiently adapt to the purpose of the study. In addition, this project aims to prevent the passage of light in the system so that only the LED emits light in order to reduce interference that could harm the progress of the experiment. Fig. 36 shows the arrangement of the colorimeter with the structure created by 3D printing.

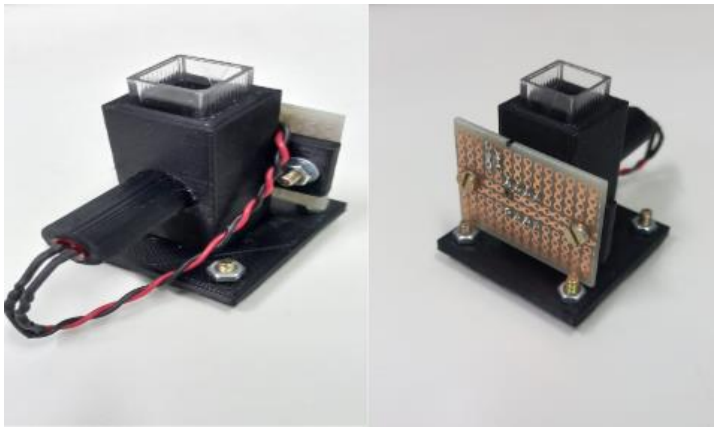

Fig. 40 Device made by 3D printing that holds the colorimeter.

IV. Mission Concept of Operations Overview

A. Ignition

The ignition phase starts after the countdown is over and the ignition is fired. The propellant grains start to burn and with it the pressure and temperature both rapidly increase in the combustion chamber. The chamber`s thermical protection mitigates the heat transferred to the fuselage, allowing the fiberglass to maintain its mechanical properties. At this point the motor`s design is put to test, as the pressure increases, chamber, bulkhead and nozzle must have been well designed to sustain the pressure.

On another part of the rocket avionics and payload are already active, receiving and storing ground data. The pressure increases until it reaches operation pressure, and the ignition phase is over.

B. Liftoff

When the combustion chamber reaches operation pressure, combustion gases are expelled from the motor`s nozzle and the rocket is accelerated, increasing in speed and beginning its movement guided by the launch rail.

During this initial movement, little has changed to the avionics and payload subsystems, which should still be detecting conditions similar to those of the operation start, except for the acceleration and velocity increase.

When the rocket is clear of the launch rail, the liftoff phase ends.

C. Propelled Flight

On this first part of the flight, as the rocket leaves the rail to a free movement, it experiences wind interference on its trajectory. Approaching a critical point, the rocket must have a minimum velocity compared to the wind so it guarantees a stable flight and the right direction.

In this phase, the rocket is constantly increasing its speed until the motor's thrust runs out, which means the rocket has reached its maximum velocity and the propellant burning is over. The end of the propellants burning marks the end of the propelled flight phase

D. Telemetry (3)

At the end of the propellants burning, the rocket starts to fly only on its inertia. It continues to increase in altitude even though its velocity is decreasing due to gravity and drag.

While the vehicle flies, its avionics and payload are storing and transmitting data. The avionics is acquiring and calculating quantities that will then be used to activate the recovery systems and validate the flight parameters. The payload on the other hand whereas filming the whole flight is also receiving a much larger amount of data from its cosmic ray detector, as on higher altitudes there are more and more particles to be detected.

E. Drogue parachute deployment (1)

The speed gradually decreases, until the rocket reaches the highest spot on its trajectory, which is the apogee, as can be seen in Fig. 2. As it reaches the apogee, the free flight phase comes to an end.

At the apogee and the first few moments of fall the avionics triggers the drogue parachute. The parameters received and transmitted by the avionics will indicate the beginning of the descending motion.

The fuselage and ropes from the first recovery system suffer a peak tension, as it breaks the fall, and the apogee phase ends.

The beginning of the fall is also the beginning of the Fall Directioning phase.

In this phase the vehicle starts its descending motion as the drogue parachute acts against its increase of speed without letting the wind carry the rocket too far sideways.

F. Main Parachute deployment (2)

After falling for about 2.5 km the rocket still has a considerable velocity, as the braking efficiency is not the drogue parachute's main purpose.

The avionics then triggers the main recovery system, as described in Fig. 2, intended to effectively slow down the last moments of fall with its velocity according to Table 9. The deployment of the main recovery system is the end of the fall directioning phase.

The fall velocity is decreased until reaching an appropriate speed for a safe ground hit. As soon as the rocket hits the ground, which is the gentle land stage described in Fig. 2, the operation ends.

V. Conclusion and Lessons Learned

In the construction of the ATOM III, several technical subsystems worked together to deliver a project capable of providing the study rocket with a launch that prioritizes technological innovations and flight safety. Therefore, the MXT solid propulsion engine was developed in order to withstand the increase in pressure and temperature of the combustion chamber during the burning period so that it is able to withstand the mechanical and thermal loads resulting from the launch and provide the ideal propulsion parameters. In addition, the structures and aerodynamics subsystems developed coupler and fuselage designs capable of remaining intact to the loads applied to the system, combined with the choice of the geometry of the ATOM III's nose cone capable of reducing the aerodynamic forces that act on the rocket. Using the COTS RRC3 altimeter, the avionics subsystem makes it possible to measure the altitude and velocity to which the rocket is submitted during the flight path. Finally, the recovery subsystem employing a gas ejection system for the main parachute and the drogue parachute allows the recovery of the rocket after the end of its trajectory, also using the 3-ring system as a considerable improvement to the project in terms of effectiveness. Therefore, the ATOM III presents satisfactory technical design conditions to establish a correct and safe flight plan.

With the entire project developed, the team was able to develop project skills by establishing new options for technological improvement capable of individually and collectively enhancing each participating member. In

addition, skills with regard to time and task management were highlighted as important points within the scope of projects in general and, more specifically, in the area of model rocketry and astronautics.

Appendix

1) System Weights, Measures and Performance Data

Table 10 Component masses

Vehicle weight	17,4 kg
Propellant weight (all)	12,0 kg
Payload weight	4,0 kg
Total liftoff weight	**33,4 kg**

Table 11 Vehicle dimensions

Total vehicle length	304.5 cm
Airframe diameter	119 mm
Fin extension	120 mm

Table 12 Performance Data

Liftoff Thrust-to-Weight Ratio	7.4
Launch Rail Departure Velocity	29.0 m/s
Minimum Static Margin During Boost	2.0
Maximum speed	262 m/s
Maximum acceleration	8 G
Target Apogee	3000 meters AGL
Predicted Apogee	2780 meters AGL

2) Project Test Reports

A) Recovery Test

In May 2022, bench tests were carried out to evaluate the total force obtained to release the main parachute and support of the system.

Satisfactory results were obtained, the system held the traction test well and the force obtained to pull the rope was sufficient for the DC Motor chosen.

Fig. 41 Static test data x Projected data

B) Static Test

The rocket engine static test consists of obtaining the thrust-time graph considering that the study engine is subjected to real operating conditions. Therefore, its importance in the validation of the project is extremely important, as it allows the validation of the propulsion systems used in the project.

The static test of the MXT engine was carried out in a large, open and suitable place for its use, respecting safety and operator distancing guidelines.

The graph represented by Fig. 42 demonstrates the thrust behavior as a function of time obtained in the static test of the MXT engine described before.

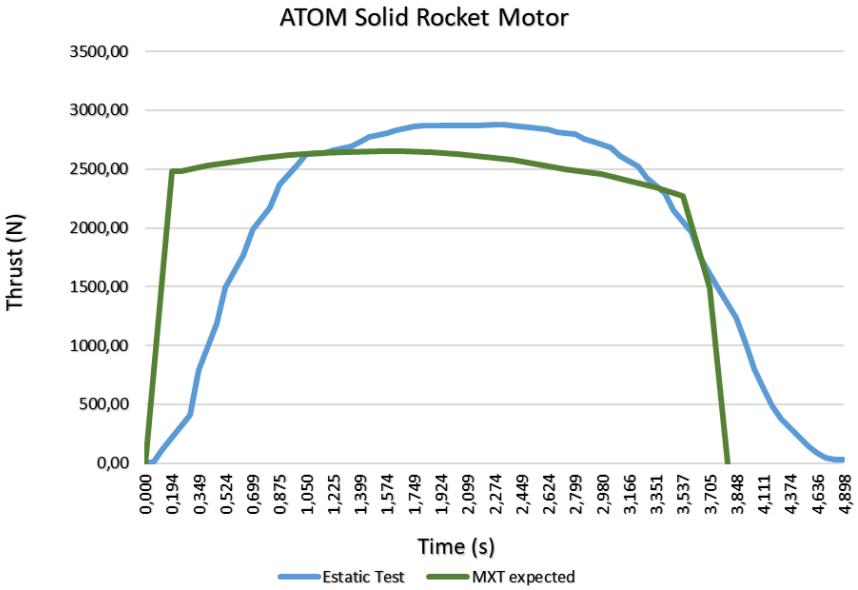

Fig. 42 Static test data.

Once the measured parameters are within the theoretical limits of the project, the MXT engine was successful in validating its objective in providing the desired propulsion system in the *ATOM III*. Therefore, the MXT engine is able to be submitted to a projected rocket launch.

Table 13 compares the practical data obtained and the theoretical pre-project data.

Table 13 Theoretical and experimental values of engines after tests

Description	Theoretical Value	Practical Value	Variation
Propeller Mass [g]	7,622	7,743 ± 1	+ 1.6 %
Propellant Grain Density	90%	91.2 ± 0.6 %	+ 2 %
Total Impulse [N·s]	9,392.52	9,142.10 ± 10	- 2.77 %
Maximum Impulse [N]	2,651	2,878 ± 10	+ 8.94 %
Specific Impulse [Isp]	125.7	120.4 ± 0.2	- 4.38 %

C) Hydrostatic test

The MXT casing, with the intents of testing and assuring the water tightness, even while coupled to the bulkhead, has been submitted to a pressure 100% greater than its maximum operating pressure, that is, to 1000 psi. Also, a visual inspection was also conducted on the parts.

We, supported by the test results, hereby conclude that our sealing system successfully prevented any possible leak, and that the aluminum tube did not suffer any sort of apparent deformation. This test can be seen in Fig. 43.

Fig. 43 ATOM's Hidrostatic Test

D) Potassium Nitrate Quality Test

To verify the quality of the potassium nitrate used, a thermogravimetric analysis (TGA) was carried out. It consists of a destructive technique in the field of thermal analysis, in which the mass variation of a sample is monitored as a function of the temperature or time in a temperature-controlled environment and atmosphere. In this way, it is possible to analyze the loss or aggregation of mass to the sample at different temperatures. In the Fig. 44, the wet Potassium Nitrate was analyzed. The result in red indicates that the sample was indeed still wet, since at about 250ºC, a loss of mass occurred.

In Fig. 45, Potassium Nitrate was analyzed after the drying process. The result in red symbolizes that the mass practically did not change as a function of the increase in temperature. Because of that, it is possible to confirm that the potassium nitrate is really dry and ready to be used in the manufacture of the propellant.

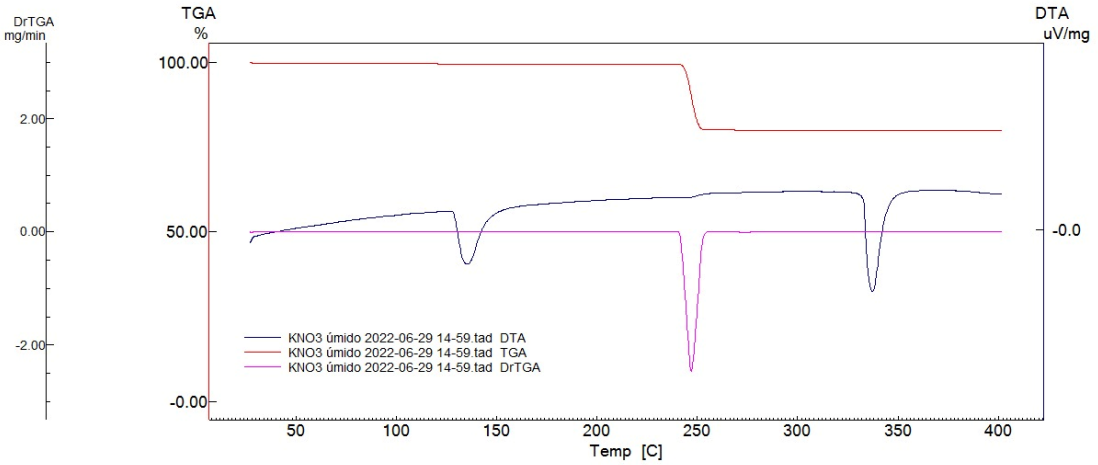

Fig. 44 Potassium Nitrate analysis.

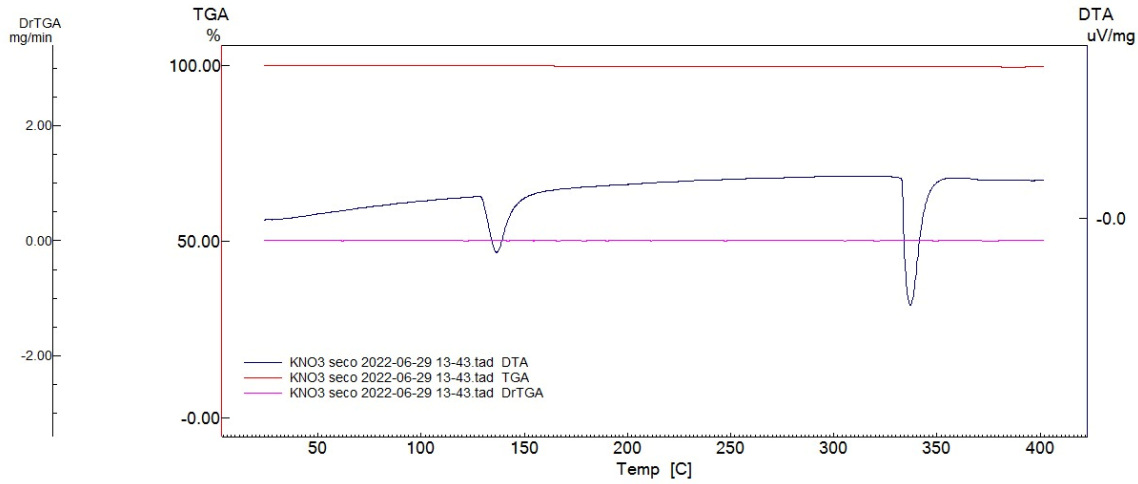

Fig. 45 Potassium Nitrate after the drying process.

E) Flight Test

The GFRJ conducted a full flight test demonstration on June 22th, 2018. Members traveled to Las Cruces, New Mexico to go through pre-launch procedure and witness our rocket take flight during Spaceport America Cup 2018. *ATOM* was vertically integrated on a 6 meters rail angled at 85 degrees from horizontal. Winds were approximately 3-4 m/s. The rocket flew straight and true. Upon main parachute and drogue deployment at the same time, the team was not able to receive an active GPS signal. The launch vehicle sustained internal damage but not external and was deemed re-flyable.

The team also conducted a demonstration flight of the second version of the rocket (*ATOM II*). The flight occurred on August 11th, 2019, reaching 2561 meters.

3) Hazard Analysis

Team	**Rocket/Project Name**	**Date**	
GFRJ	*ATOM III*	01/07/2022	
Hazardous material	**Possible Hazards**	**Mitigation Approach**	**Risk of injury after mitigation**
Propellant grain	Spontaneous combustion	Avoid keeping propellant grain in closed containers that may be pressurized in case of combustion	Low
		Avoid exposing it to intense heat for long periods of time	
		Avoid using polyester coats as preparing the grain. (Avoiding static charges)	
Black Powder	Burn or explode	Be careful with static charges	Low
		Be careful with electronic devices and electric current near the powder	

4) Risk Assessment

Team	**Rocket/Project Name**	**Date**		
GFRJ	*ATOM III*	01/07/2022		
Hazard	**Possible Causes**	**Risk of Mishap and Rationale**	**Mitigation Approach**	**Risk of injury after mitigation**
Explosion of solid-propellant rocket motor during launch with blast or flying debris causing injury	Cracks or Air Bubbles in propellant grain	Medium: student-built motor with limited testing and nondestructive evaluation capability	Pressure test motor case to 2 times maximum operating pressure	Low
	Gaps between propellant sections and/or nozzle		Visually inspect motor grains for cracks and debonds during and after assembly Extra propellant grains in order to choosing the most appropriate for the operation	
	Chunk of propellant or inhibitor breaking off and plugging nozzle		Use of ductile material for motor case	
	Motor case unable to contain normal operating pressure		Inspect motor case for damage during final assembly before launch	

	Motor closures fail to hold		Only essential personnel in launch crew	
			Launch crew 200 feet from rocket at launch, behind barrier	
Rocket does not ignite when command is given, but does ignite when team approaches to troubleshoot	Ignition system malfunction	Medium; ignition system is student-built, and ignition is not always visible at first sight	Multiple testing of ignition system	Low
	Activation squib felt from rocket motor		In case of ignition failure, not approaching the rocket for a safety amount of time (5 to 10 minutes)	
	Ignition operation not properly executed		Launch operation printed and at hand	
Recovery system deploys during assembly or pre-launch and causes injury	Recovery activation malfunction	Low; both deployment systems are commercial	Avionics only activated when "remove before flight" is removed	Low
Rocket deviates from nominal flight path, comes in contact with personnel	Manufacturing is not faithful to design	High; motor and fuselage are student-built with the affordable tools and methods Wind and weather conditions hard to foresee and simulate	Simulations were made after the manufacturing with real data, presenting little the deviation from the expected results	Medium
	Rocket motor does not reach the desired efficiency		Static fire tests made point out a close to estimated efficiency	
	Vehicle does not reach minimum stability velocity due to windy conditions		Research on usual weather conditions at place of launch enable more reliable simulation results	
			Operation includes calling personnel's attention to the launch in order to ease possible reactions to this hazard	
Low Recovery system partially deploys, rocket or payload encounter personnel	Avionics malfunction	Medium; complex operation of parachute folding, inserting and activating	Redundancy with commercial equipment rises the reliability of the system	Low
	Structure not sustaining enough		Tests made on similar structure	

	tension		guaranteed sustaining this amount of tension	
	Parachute or strings do not sustain enough tension		Commercial parachute design by professional parachute manufacturer rises the reliability of the project	
	Parachute gets stuck in the fuselage		Folding and insering procedures recommended by the manufacturer	
Recovery system fails to deploy, rocket or payload encounter personnel	Avionics malfunction	Low; redundant activation system	Redundancy with commercial equipment rises the reliability of the system	Low

5) Assembly, Preflight, Launch, and Recovery Checklists

Materials Checklist		
Action number	**Action**	**Check**
1	**External structure**	-
2	Three fuselage tubes	-
3	Attach nose's tip	-
4	Hole alignment	-
5	Fin integrity	-
6	Fin's attachment	-
7	Four couples	-
8	Screws	-
	Propulsion	
1	Motor tube integrity	-
2	Thermal liner	-
3	Propellents	-
4	Number of bolts	-
5	O-rings	-
6	Nozzle	-
	Recovery	
1	Strings	-
2	Main parachute	-
3	Drogue	-
4	Gunpowder	-
	Avionics	
1	PCB	-
2	Avionic’s case	
3	Altimeter	-

4	Antenna	-
5	Batteries	-
6	RBF	-
	Payload	
1	Structure	-
2	Experiments	-
3	Payload's eletronics	-

Assembly Checklist		
Action numbers	**Action**	**Check**
1	Check the Experiments Payload	-
2	Insert payload's "remove before flight" pin	-
3	Structure Payload insertion on its module	-
4	Main parachute anchoring on payload module	-
5	Avionics coupler preparation	-
6	Avionics security key check	-
7	Main parachute powder preparation and allocation	-
8	Drogue parachute powder preparation and allocation	-
9	Main parachute anchoring and allocation	-
10	Connection of drogue parachute module with avionics coupler	-
11	Drogue parachute anchoring	-
12	Connection of drogue parachute module with avionics coupler	-
13	Insert avionics "remove before flight" pin and turn off security key*	-
14	Drogue parachute allocation	-
15	Anchoring drogue parachute on motor module	-
16	Connection of motor and drogue parachute module	-
17	Insert propellant in motor case	-
18	Nozzle enclosing**	-
19	Motor final check and assembly	-
20	Motor insertion***	-
21	Motor anchoring ring insertion	-
Preflight Checklist		
Action number	**Action**	**Check**
1	Check for required personal protective equipment	-
2	Check for green range status flag	-
3	Take rocket to launch pad	-
4	Rocket position on launch rail correctly	-
5	Arming avionics	-
6	Verify altimeter beep code	-
7	Check range manager's permission to install	-

	motor igniters	
8	Motor igniter inserted and secure	-
9	Evacuate launch area	-
Launch Checklist		
Action number	**Action**	**Check**
1	Wait for MCO,RSO and LCO "go for flight" messages	-
2	Wait for LCO's final countdown	-
3	Ignition	-

Engineering Drawings

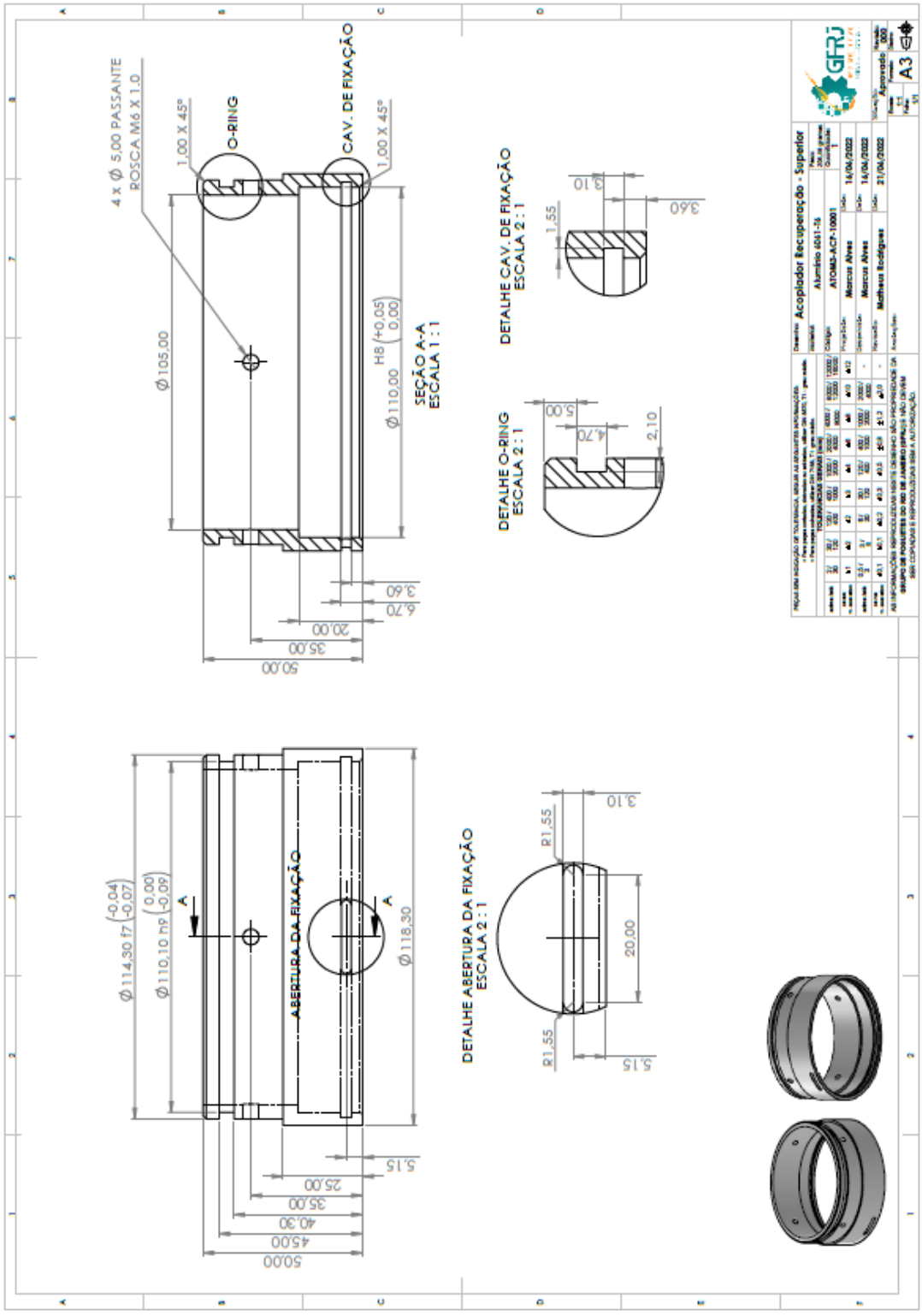

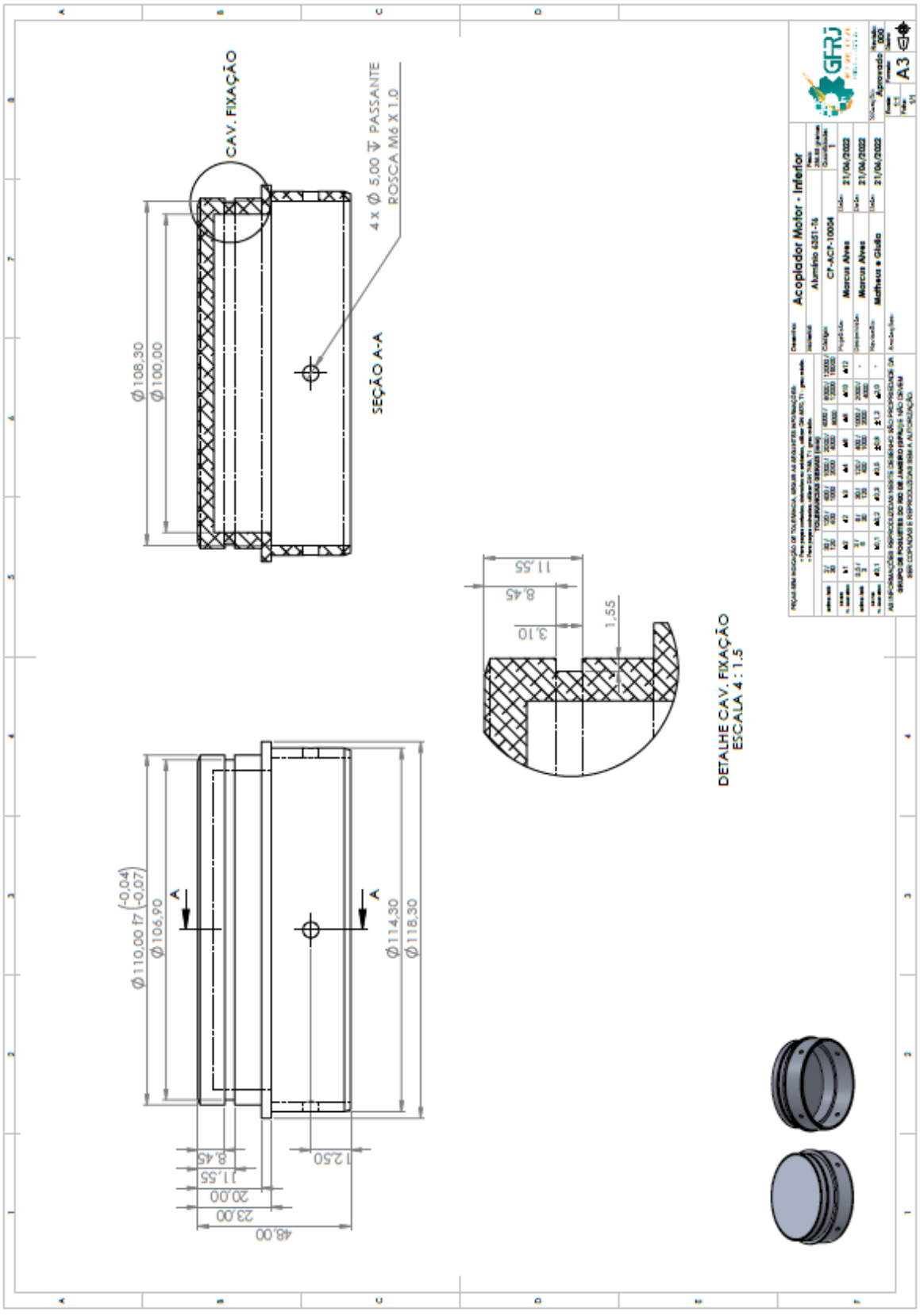
CAV. FIXAÇÃO
4 x Ø 5,00 ↧ PASSANTE
ROSCA M6 X 1.0
SEÇÃO A-A
Ø108,30
Ø100,00
DETALHE CAV. FIXAÇÃO
ESCALA 4 : 1.5
11,55
8,45
3,10
1,55
Ø110,00 f7 (-0,04 -0,07)
Ø106,90
Ø114,30
Ø118,30
12,50
8,45
11,55
20,00
23,00
48,00
Acoplador Motor - Inferior
Alumínio 6351-T6
CF-ACP-10004
Marcos Alves
Marcos Alves
Matheus e Giulio
21/04/2022
A3

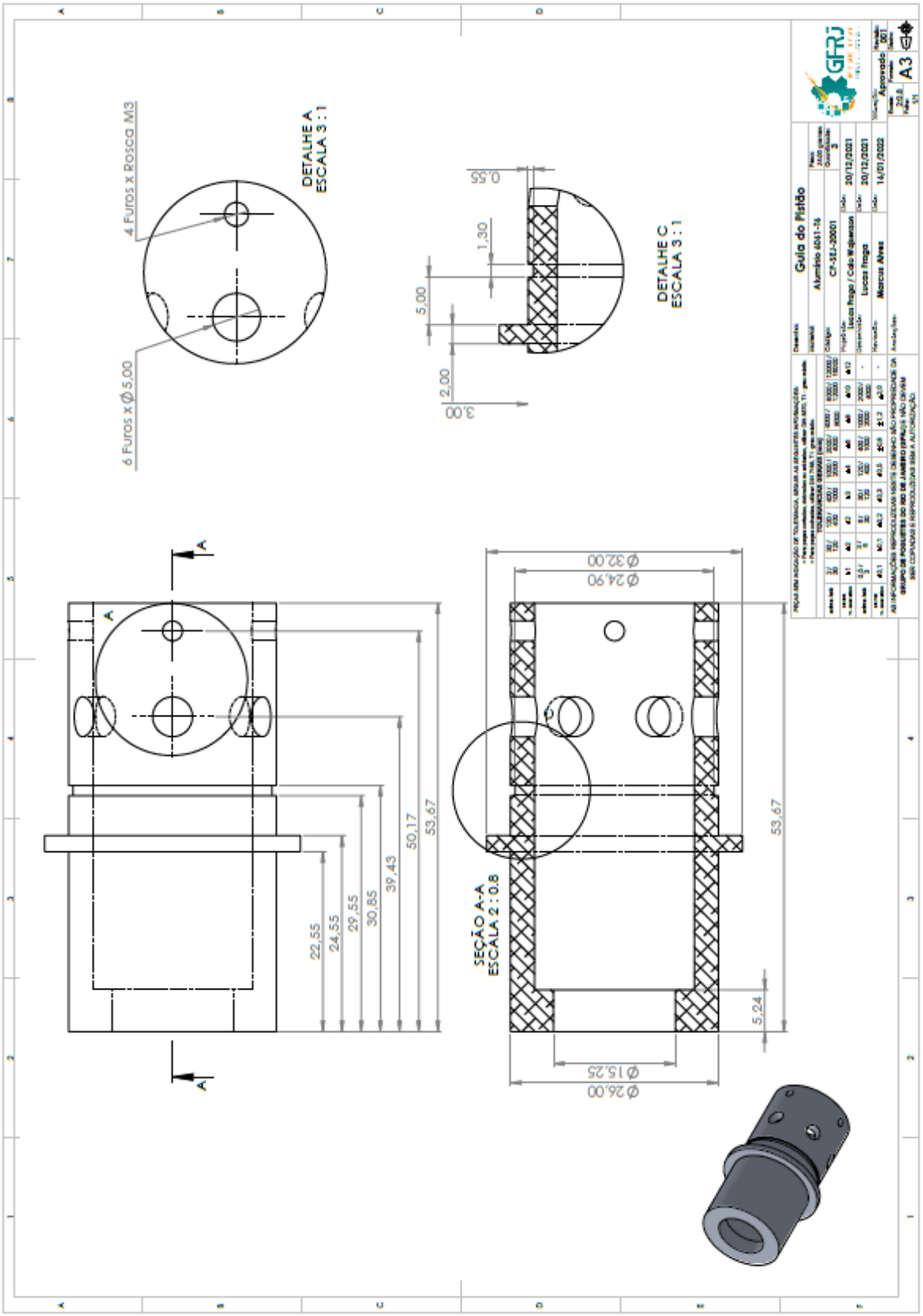
4 Furos x Rosca M3
6 Furos x Ø5,00
DETALHE A
ESCALA 3 : 1
0,55
1,30
5,00
2,00
3,08
DETALHE C
ESCALA 3 : 1
Guia do Pistão
Alumínio 6061-T6
CP-SEU-20001
Lucas Fraga / Cela Wagenaar
Lucas Fraga
Marcus Alves
20/12/2021
20/12/2021
14/01/2022
A3
Ø 32,00
Ø 24,90
Ø 26,00
Ø 15,25
53,67
5,24
22,55
24,55
29,55
30,85
39,43
50,17
53,67
SEÇÃO A-A
ESCALA 2 : 0,8

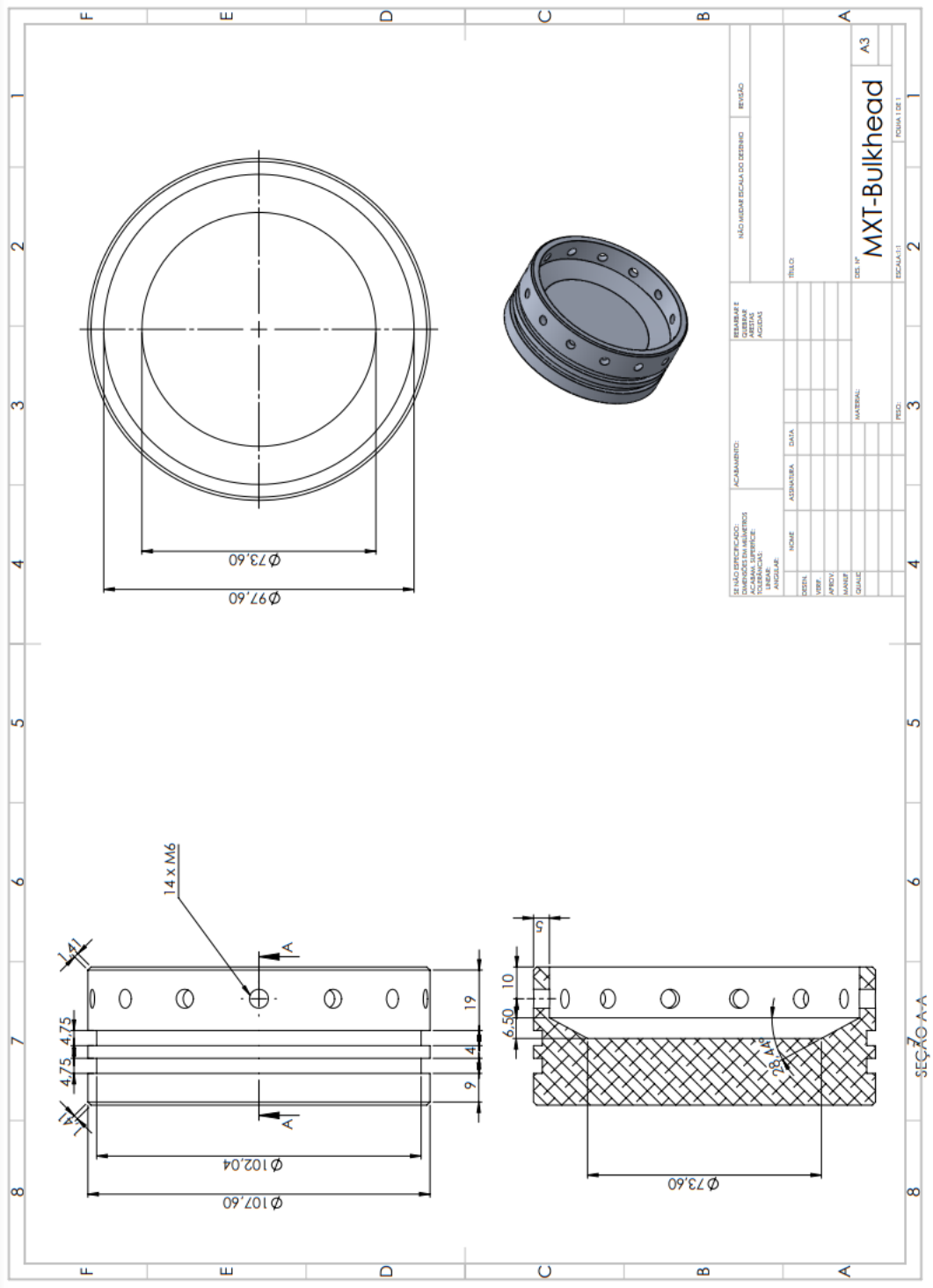
MXT-Bulkhead
A3
Ø97,60
Ø73,60
14 x M6
4,75
4,75
19
4
9
Ø102,04
Ø107,60
10
6,50
45°
Ø73,60
SEÇÃO A-A

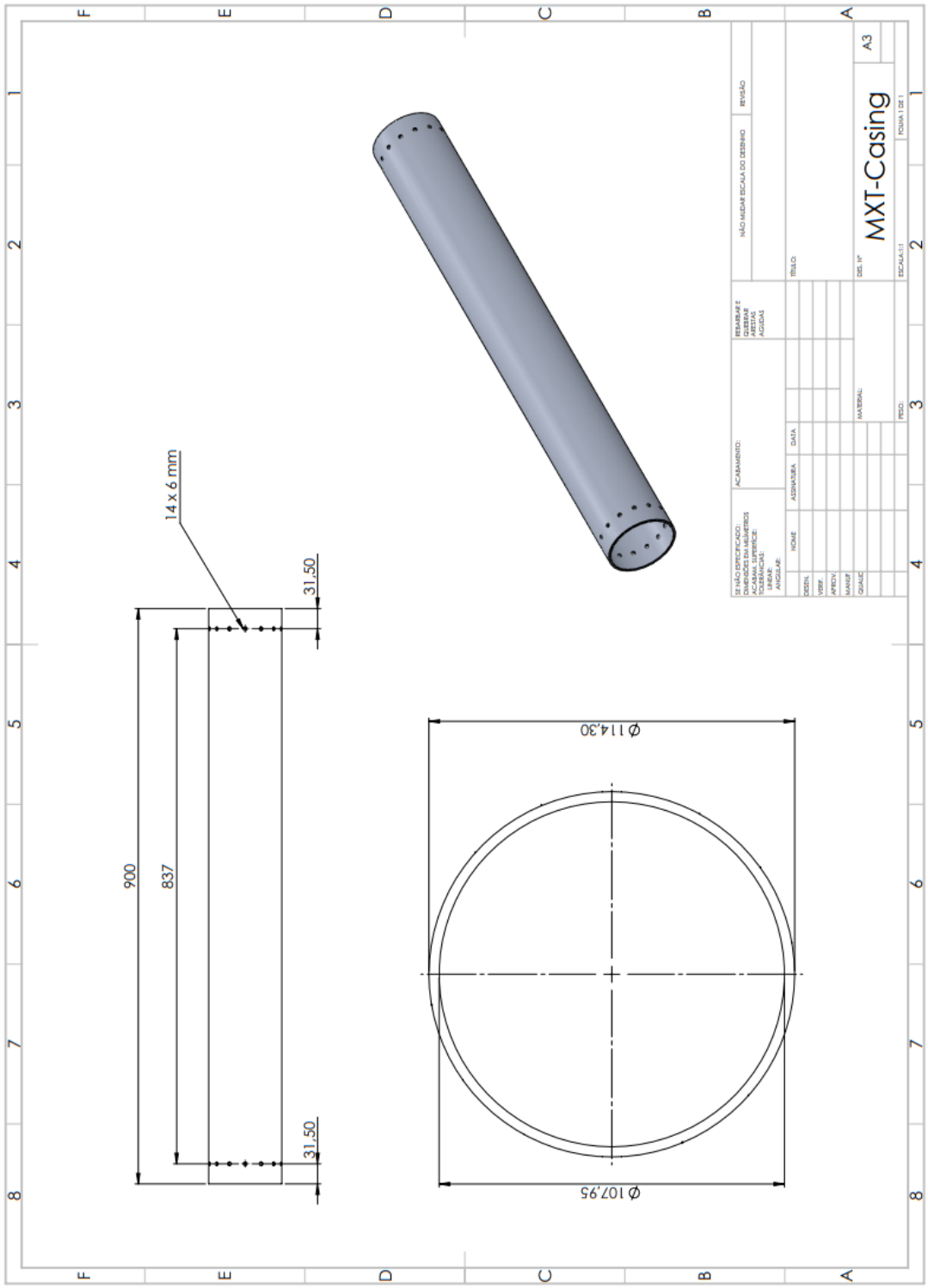
MXT-Casing
A3
14 x 6 mm
31,50
900
837
31,50
Ø114,30
Ø107,95

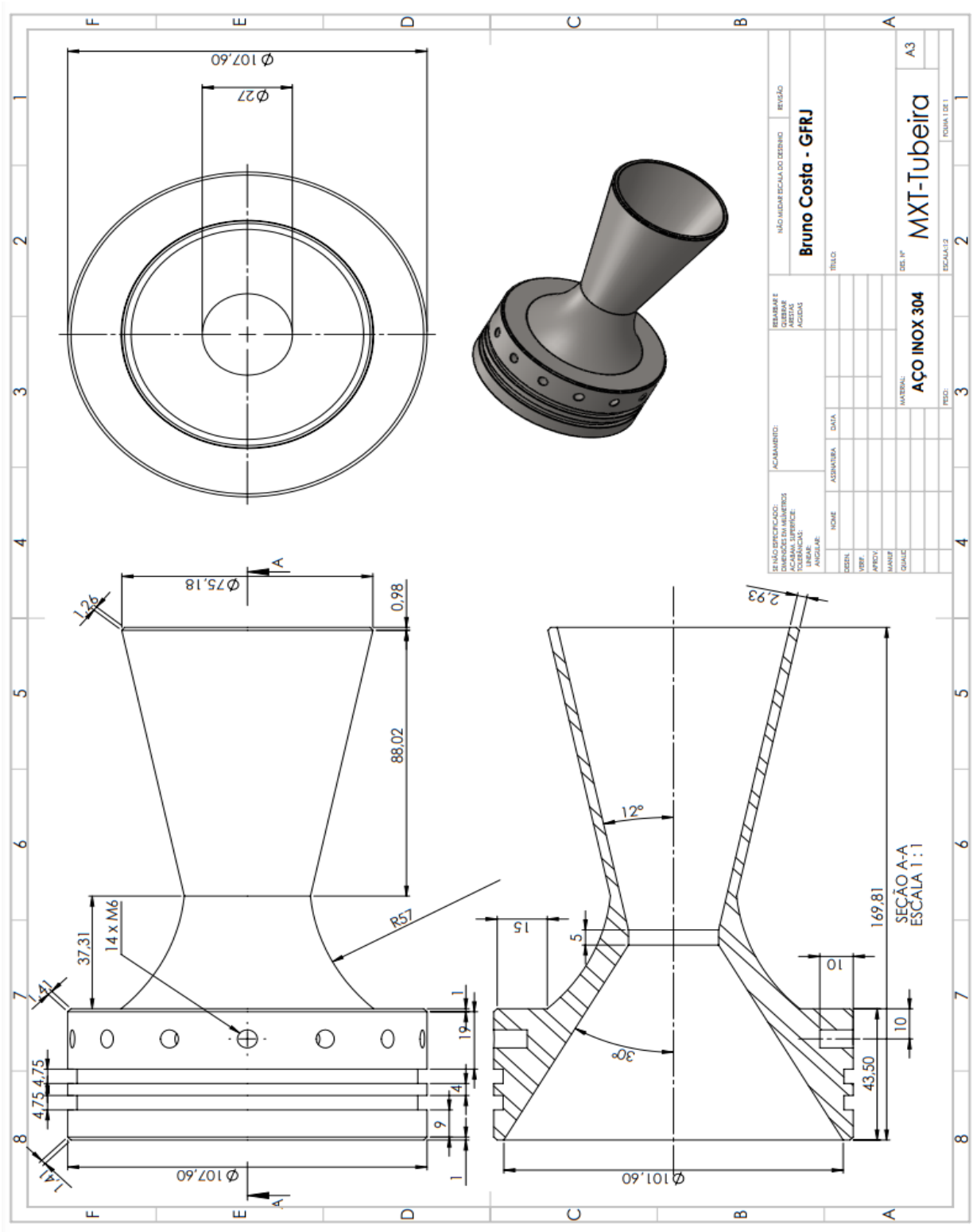
Ø107,60
Ø27
Ø75,18
A
1,26
0,98
88,02
37,31
14 x M6
R57
4,1
4,75
4,75
19
4
9
1
Ø107,60
A
2,93
12°
30°
15
5
10
169,81
10
43,50
Ø101,60
SEÇÃO A-A
ESCALA 1 : 1
Bruno Costa - GFRJ
MXT-Tubeira
A3
AÇO INOX 304

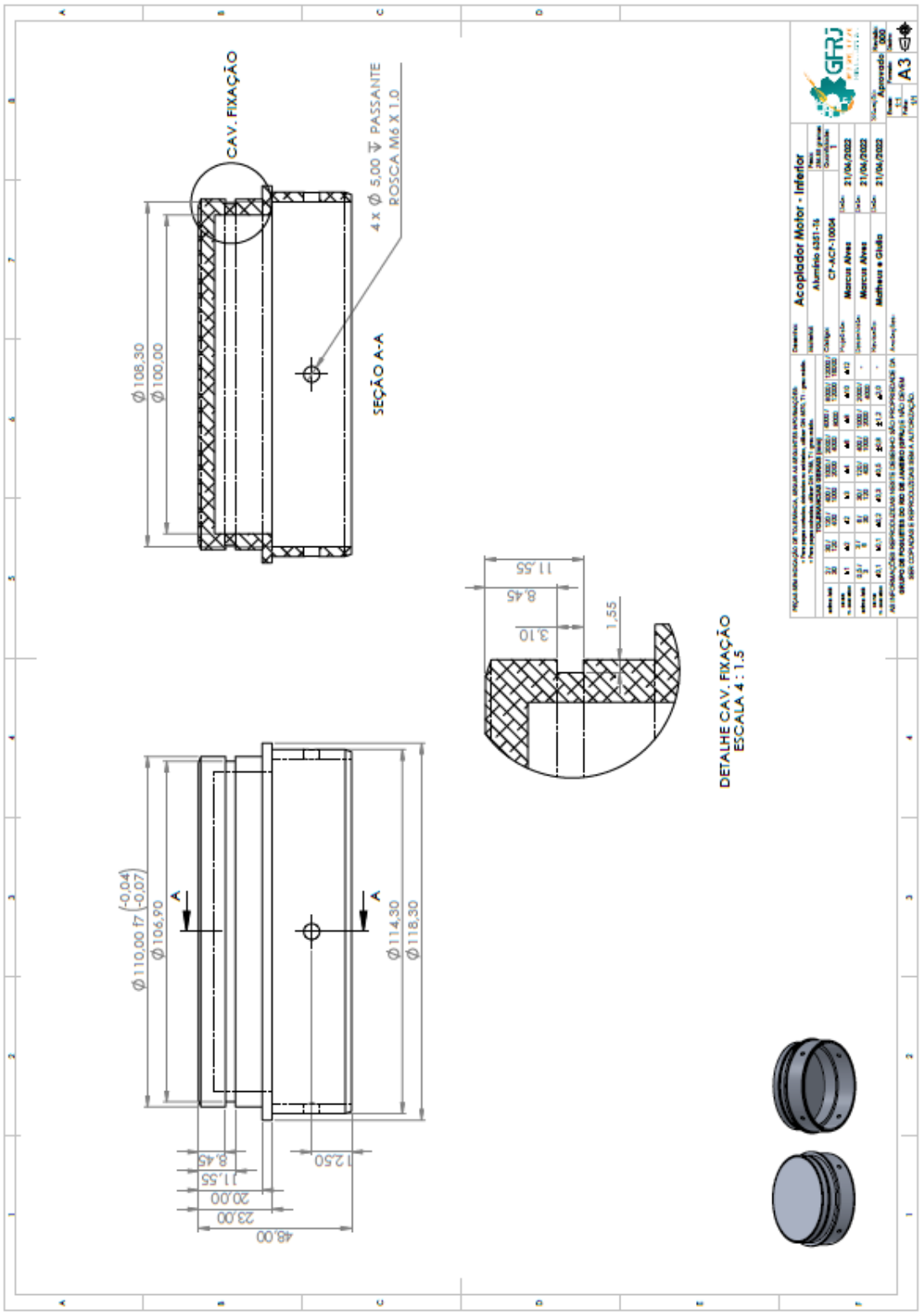
CAV. FIXAÇÃO
4 x Ø 5,00 ↧ PASSANTE
ROSCA M6 X 1.0
SEÇÃO A-A
Ø108,30
Ø100,00
DETALHE CAV. FIXAÇÃO
ESCALA 4 : 1.5
11,55
8,45
3,10
1,55
Ø110,00 f7 (-0,04 -0,07)
Ø106,90
Ø114,30
Ø118,30
12,50
8,45
11,55
20,00
23,00
48,00
Acoplador Motor - Inferior
Alumínio 6351-T6
CF-ACP-10004
Marcos Alves
Matheus e Giulia
31/04/2022
A3

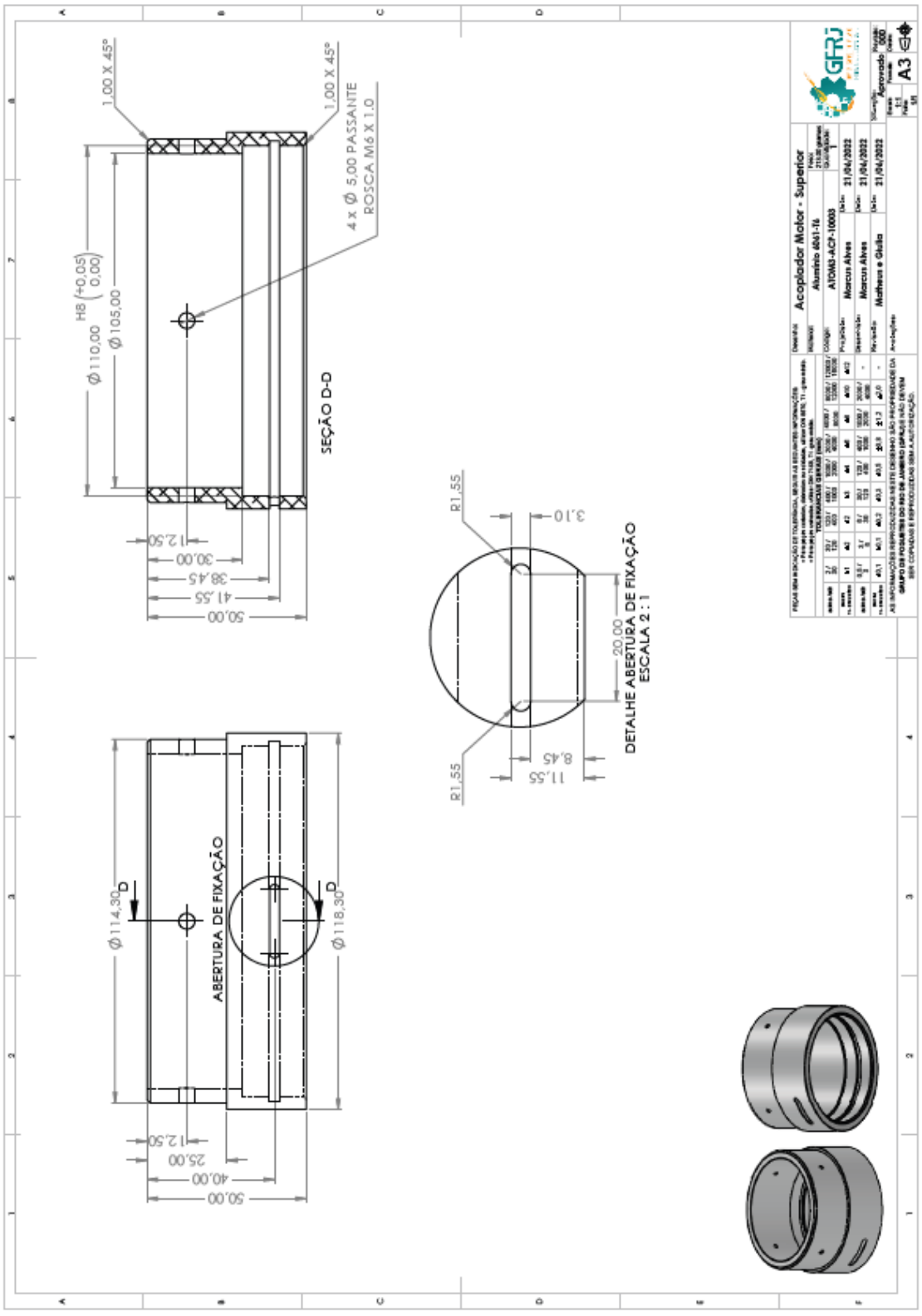
1,00 X 45°
1,00 X 45°
4 x Ø 5,00 PASSANTE
ROSCA, M6 X 1.0
SEÇÃO D-D
H8 (+0,05 0,00)
Ø110,00
Ø105,00
12,50
30,00
38,45
41,55
50,00
R1,55
3,10
20,00
11,55
8,45
R1,55
DETALHE ABERTURA DE FIXAÇÃO
ESCALA 2 : 1
ABERTURA DE FIXAÇÃO
Ø114,30
Ø118,30
12,50
25,00
40,00
50,00
Acoplador Motor - Superior
Alumínio 6061-T6
ATOM3-ACP-10003
Marcus Alves
Marcus Alves
Matheus e Giulia
21/04/2022
A3

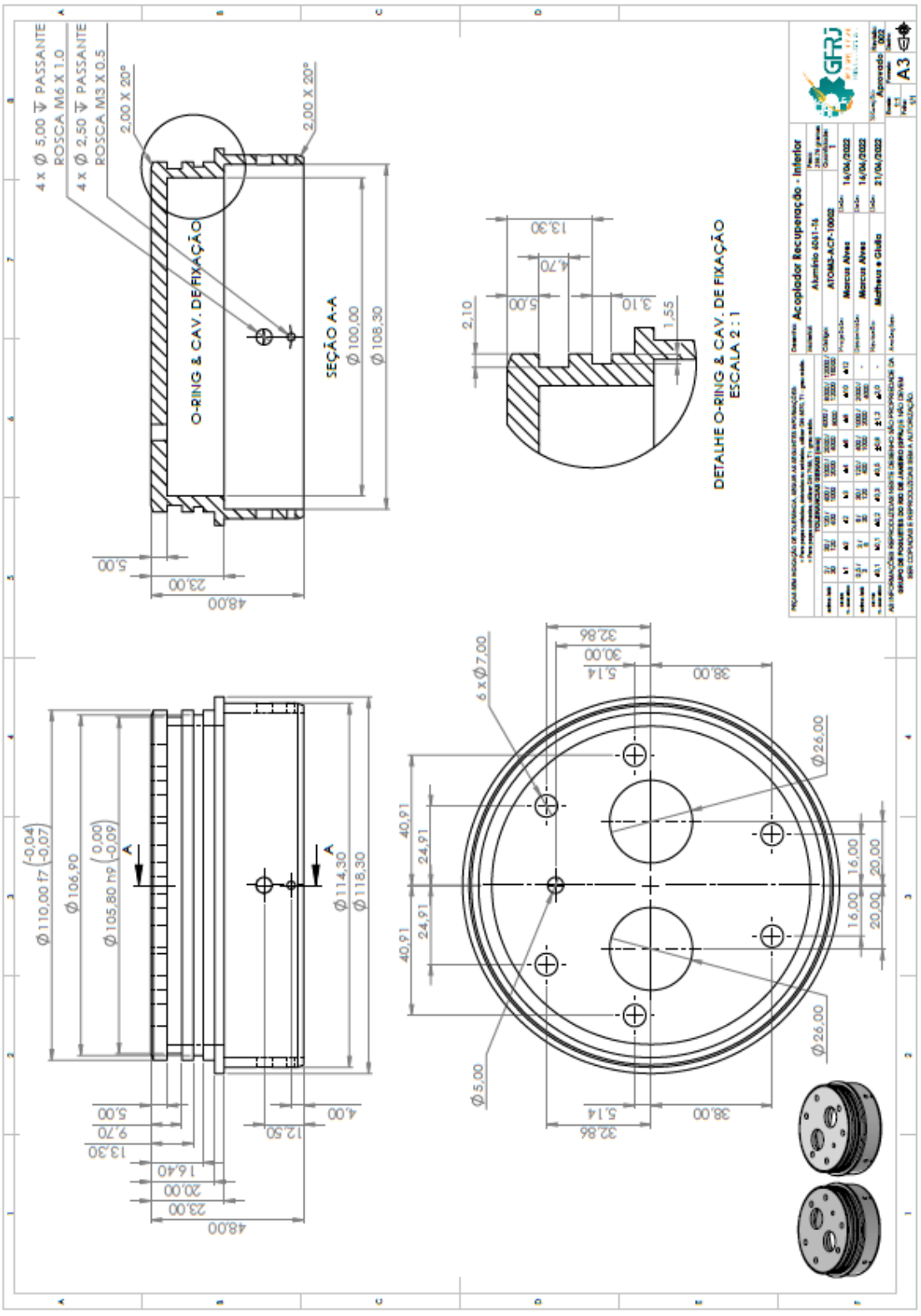
4 x Ø 5,00 ↧ PASSANTE
ROSCA M6 X 1.0
4 x Ø 2,50 ↧ PASSANTE
ROSCA M3 X 0.5
2,00 X 20°
2,00 X 20°
O-RING & CAV. DE FIXAÇÃO
SEÇÃO A-A
Ø100,00
Ø108,30
5,00
23,00
48,00
DETALHE O-RING & CAV. DE FIXAÇÃO
ESCALA 2 : 1
13,30
4,70
5,00
3,10
1,55
2,10
Ø110,00 f7 (-0,04 -0,07)
Ø106,90
Ø105,80 h9 (0,00 -0,09)
Ø114,30
Ø118,30
A
A
5,00
9,70
13,30
16,40
20,00
23,00
48,00
12,50
4,00
6 x Ø7,00
32,86
30,00
5,14
38,00
Ø26,00
40,91
24,91
16,00
20,00
Ø5,00
Acoplador Recuperação - Inferior
Alumínio 6061-T6
ATOM3-ACP-10002
Marcos Alves
Marcos Alves
Matheus e Otávio
14/04/2022
14/04/2022
21/04/2023
GFRJ
A3

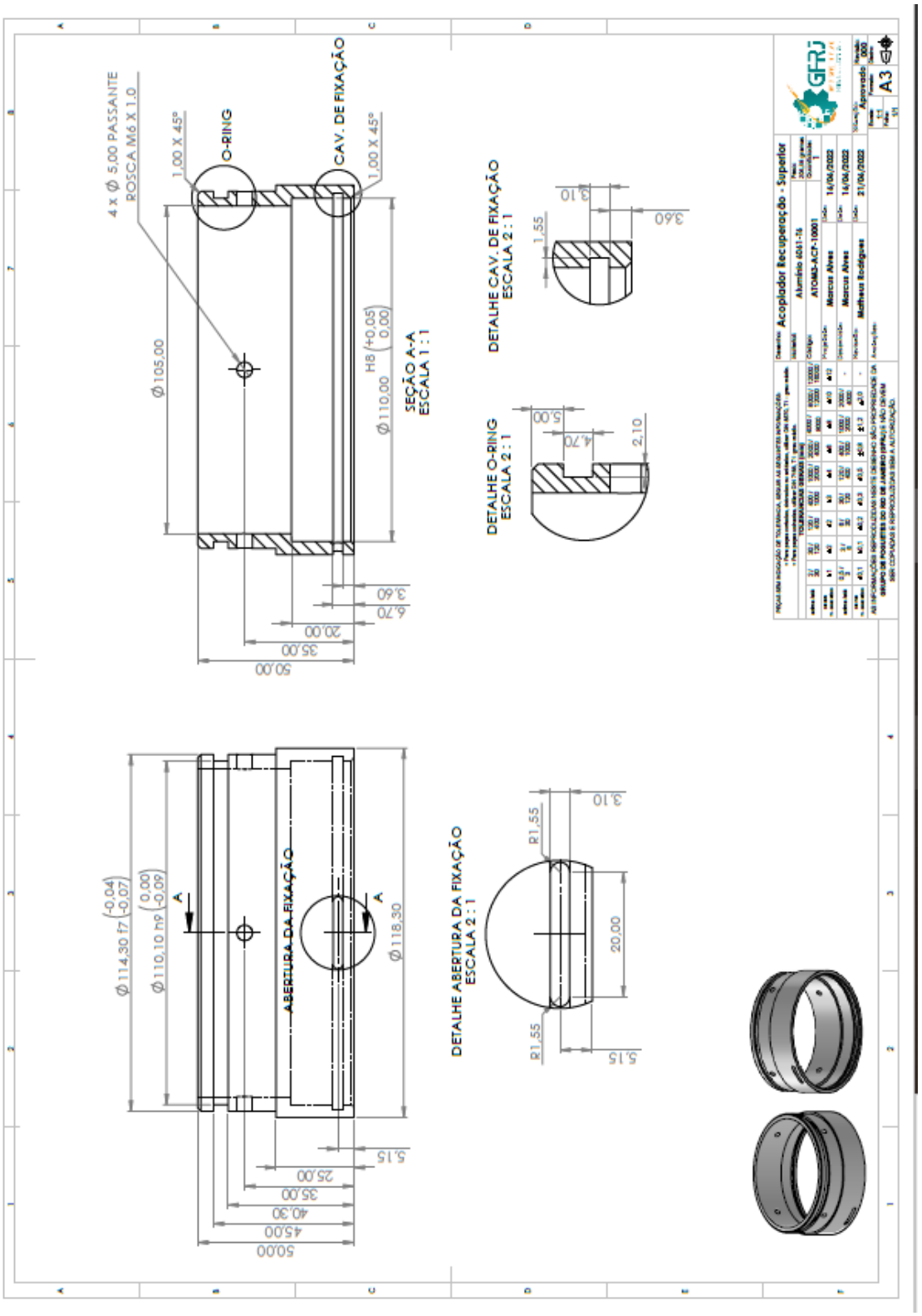
4 x Ø 5,00 PASSANTE
ROSCA M6 X 1.0
1,00 X 45°
O-RING
CAV. DE FIXAÇÃO
1,00 X 45°
Ø105,00
H8 (+0,05 0,00)
Ø110,00
SEÇÃO A-A
ESCALA 1 : 1
3,60
6,70
20,00
35,00
50,00
DETALHE CAV. DE FIXAÇÃO
ESCALA 2 : 1
3,10
1,55
3,60
DETALHE O-RING
ESCALA 2 : 1
5,00
4,70
2,10
Ø114,30 f7 (-0,04 -0,07)
Ø110,10 h9 (0,00 -0,09)
A
A
ABERTURA DA FIXAÇÃO
Ø118,30
5,15
25,00
35,00
40,30
45,00
50,00
DETALHE ABERTURA DA FIXAÇÃO
ESCALA 2 : 1
R1,55
3,10
20,00
R1,55
5,15
Acoplador Recuperação - Superior
Alumínio 6061-T6
ATOMS-ACP-10001
Marcos Alves
14/04/2022
Marcos Alves
14/04/2022
Matheus Rodrigues
21/04/2022
A3

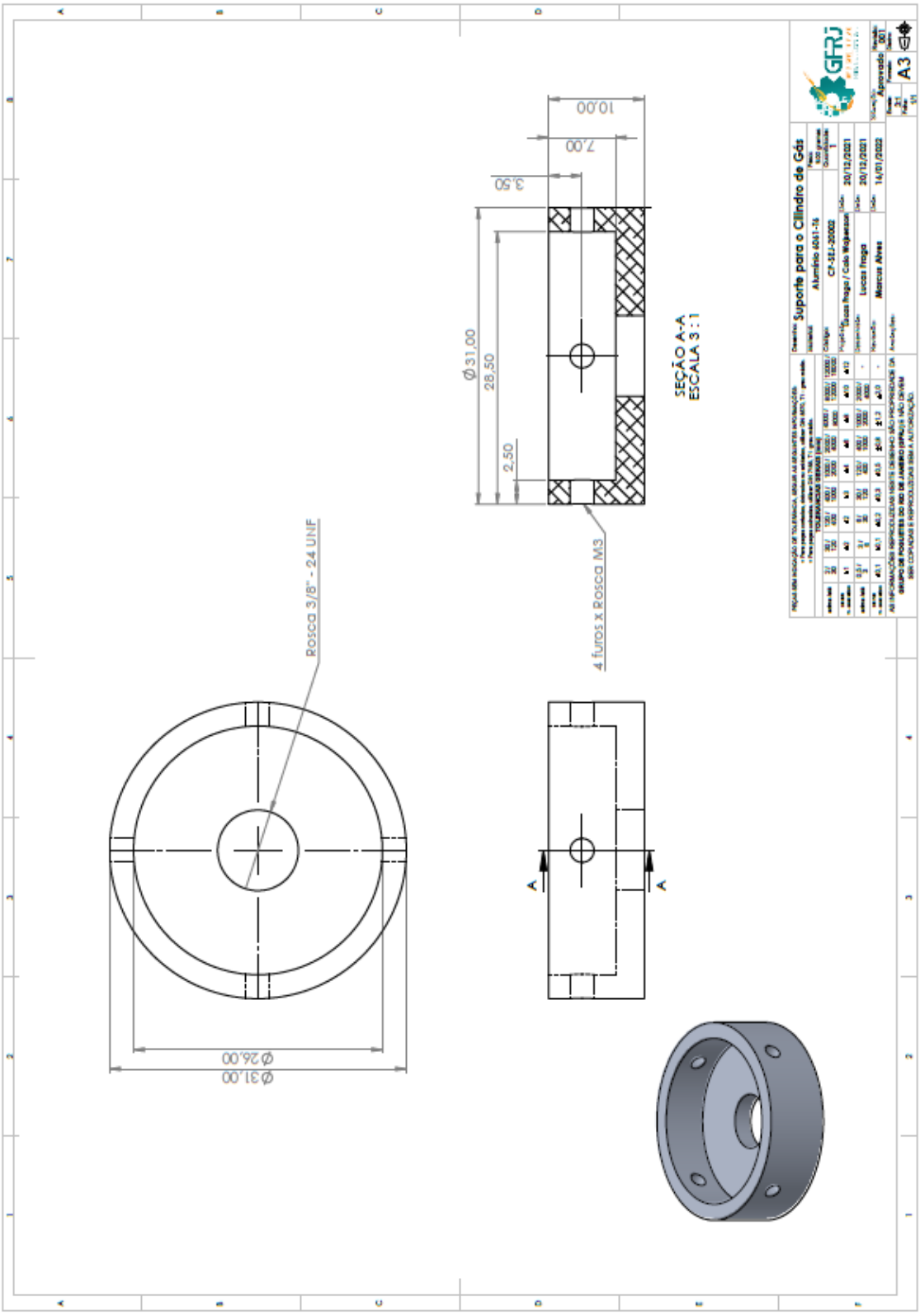
10,00
7,00
3,50
Ø31,00
28,50
2,50
SEÇÃO A-A
ESCALA 3 : 1
4 furos x Rosca M3
Rosca 3/8" - 24 UNF
Ø31,00
Ø26,00
A
A
Suporte para o Cilindro de Gás
Alumínio 6061-T6
CF-SS2-25002
Lucas Fraga / Caio Wajsenzon
20/12/2021
Lucas Fraga
20/12/2021
Marcos Alves
14/01/2022
A3

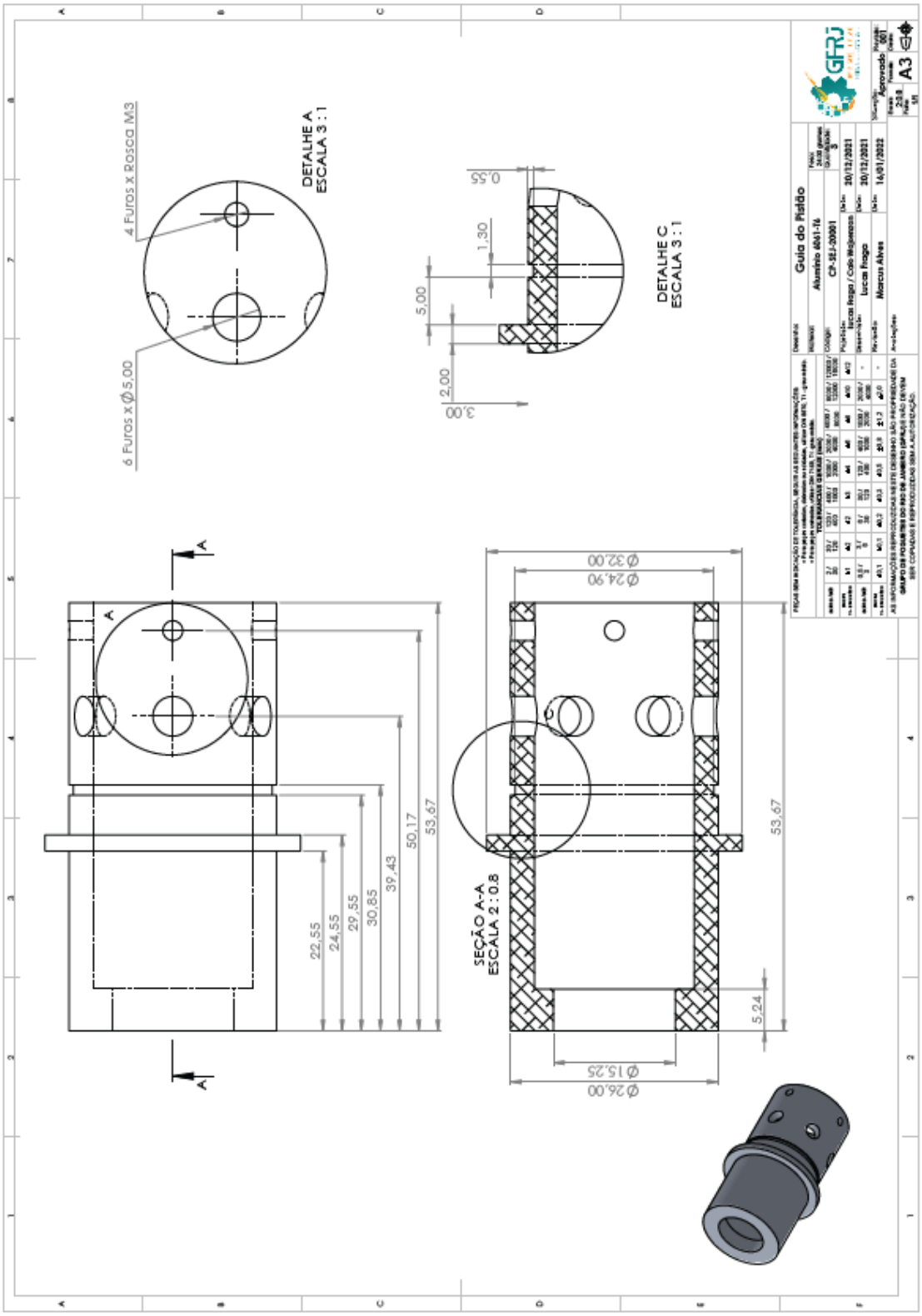
4 Furos x Rosca M3
6 Furos x Ø5,00
DETALHE A
ESCALA 3 : 1
0,55
1,30
5,00
2,00
3,00
DETALHE C
ESCALA 3 : 1
A
A
22,55
24,55
29,55
30,85
39,43
50,17
53,67
Ø32,00
Ø24,90
53,67
5,24
Ø15,25
Ø26,00
SEÇÃO A-A
ESCALA 2 : 0.8
Guia do Pistão
Alumínio 6061-T6
CP-SEI-20001
30/12/2021
30/12/2021
14/01/2022
Marcos Alves
A3

References

[1] Callister, William D., Jr.; Rethwisch, David G., *Ciência e Engenharia de Materiais: Uma Introdução*, 9th ed., LTC, Rio de Janeiro, 2018, pp. 154, 665.

[2] Hibbeler, R. C., *Resistência dos materiais*, 7th ed., Pearson, São Paulo, 2012, pp. 1, 567.

[3] Mishra, D. P., *Fundamentals of Rocket Propulsion*, 1st ed., CRC Press, United States, 2020, pp. 1, 462.

[4] Sutton, George P.; Biblarz, Oscar, *Rocket Propulsion Elements*, 8th ed., Wiley, Unitec States, 2010, pp. 1, 764.

[5] Çengel, Yunus A.; Cimbala, John M., *Mecânica dos fluidos: Fundamentos e aplicações*, 3rd ed., McGraw Hill, Porto Alegre, 2015, pp. 1, 933.

[6] Çengel, Yunus A., Ghajar, Afshin J., *Transferência de Calor e Massa: Uma abordagem prática*, 4th ed., McGraw Hill, Porto Alegre, 1984, pp. 1, 409.

[7] Ponomarenko, A., "*RPA: Tool of Liquid Propellant Rocket Engine Analysis*", 2010.

[8] RICHARD NAKKA'S EXPERIMENTAL ROCKETRY WEB SITE. Amateur Experimental Rocketry. Available in: https://www.nakka-rocketry.net/. Accessed in: 30 jun. 2022.